HOST UNIVERSITY: The University of Edinburgh – The University of Queensland

FACULTY: School of Engineering – The Faculty of Engineering, Architecture and Information Technology

DEPARTMENT: Institute of Infrastructure and Environment – School of Civil Engineering

Academic Year 2017-2019

INFLUENCE OF SUSTAINED STRESS AND HEATING CONDITIONS ON THE OCCURRENCE OF FIRE-INDUCED CONCRETE SPALLING

Andrei Lazouski

Promoters:

Dr Cristian Maluk

Prof. Luke Bisby

Master thesis submitted in the Erasmus+ Study Programme

International Master of Science in Fire Safety Engineering

Disclaimer

This thesis is submitted in partial fulfillment of the requirements for the degree of The International Master of Science in Fire Safety Engineering (IMFSE). This thesis has never been submitted for any degree or examination to any other University/programme. The author(s) declare(s) that this thesis is original work except where stated. This declaration constitutes an assertion that full and accurate references and citations have been included for all material, directly included and indirectly contributing to the thesis. The author(s) gives (give) permission to make this master thesis available for consultation and to copy parts of this master thesis for personal use. In the case of any other use, the limitations of the copyright have to be respected, in particular with regard to the obligation to state expressly the source when quoting results from this master thesis. The thesis supervisor must be informed when data or results are used. The main body of the thesis contains 15015 words.

Read and approved,

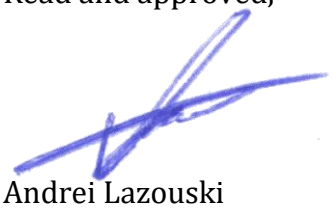

Andrei Lazouski
30/04/2019

Abstract

Experimental research of propensity to spalling of concrete samples under compressive load and radiant heating was conducted. The samples with dimensions 300×300×220 mm were cast in two groups: one group of samples included 1.6 kg/m^3 of polypropylene fibres in the mix and the other one did not. The samples were simultaneously exposed to two types of external actions: radiant heating and sustained mechanical compressive loading. The influence of different heating regimes involving parametric temperature-time curves described in Eurocode, the level of sustained mechanical compressive loading and the inclusion of polypropylene fibres in the concrete mix on the propensity of concrete samples to spalling were studied in the research.

Heating regimes were varied by changing the opening factor in the procedure defined by Eurocode from $O = 0.0415\ m^{1/2}$ up to the maximum allowed value of $O = 0.2\ m^{1/2}$.

Levels of sustained mechanical loading were varied from 19% to 53% of the ultimate compressive strain of concrete. The level of loading was controlled by the glued strain gauges on the exposed to heat faces of concrete samples.

The analysis of experimental results showed that sustained mechanical compressive loading enhances the propensity of concrete samples to spalling at the same heating regimes. The increased rate of heating changes not only the type of spalling from one-time to progressive, but also requires less energy for a spalling event to occur. As a result of the analysis, a diagram which summarizes the conditions of heating rates and loading levels was created.

Apart from that, the inclusion of 1.6 kg/m^3 of polypropylene fibres in the mix was proved to be an effective measure in the mitigation of propensity of concrete samples to heat-induced spalling.

Рэзюмэ

Было праведзена эксперыментальнае даследаванне схільнасці да сколвання ўзораў бетону пры сціскальнай нагрузцы і нагрэве выпраменьваннем. Узоры бетону з памерамі 300×300×220 мм былі адліты ў дзвюх групах: адна група узораў уключала 1,6 кг/м^3 поліпрапіленавых валокнаў у сумесі, а іншая – не. Узоры падвяргаліся ўздзеянню адначасова двух тыпаў знешніх уздзеянняў: прамяністага нагрэву і ўстойлівай механічнай сціскальнай нагрузкі.

У даследаванні вывучаліся ўплывы розных рэжымаў нагрэву, якія ўключаюць параметрычныя крывыя залежнасці тэмпературы ад часу, якія апісаны ў адпаведнсці Еўракодам, узроўняў ўстойлівай механічнай сціскальнай нагрузкі і ўключэння поліпрапіленавых валокнаў у бетоннай сумесі на схільнасць узораў бетону да сколвання.

Рэжымы нагрэву вар'іравалі шляхам змены каэфіцыенту праёмнаці ў парадку, вызначаным Еўракодам ад $O = 0.0415$ *м*$^{1/2}$ да максімальна дапушчальнага значэння $O = 0.2$ *м*$^{1/2}$.

Ўзроўні ўстойлівай механічнай нагрузкі вар'іраваліся ад 19% да 53% ад максімальнай адноснай дэфармацыі бетону пры сцісканні. Адпаведнасць нагрузкі кантралявалася прылепленымі тэнзадатчыкамі на гранях узораў бетону, якія падвяргаліся выпраменьванню.

Аналіз эксперыментальных вынікаў паказаў, што ўстойлівая механічная сціскальная нагрузка павялічвае схільнасць узораў бетону да сколвання пры аднолькавых рэжымах нагрэву. Павялічаная хуткасць нагрэву не толькі змяняе тып сколвання з аднаразовага да прагрэсіўнага, але таксама патрабуе менш энергіі для здзяйснення сколвання. У выніку аналізу была створана схема, на якой падагульнены ўмовы хуткасцяў нагрэву і ўзроўняў нагрузкі.

Акрамя таго, было даказана, што ўключэнне 1,6 кг/м^3 поліпрапіленавых валокнаў у бетонную сумесь з'яўляецца эфектыўнай мерай для змякчэння схільнасці узораў бетону да сколвання ад нагрэву.

ACKNOWLEDGEMENTS

I want to express my gratitude to the management board of the IMFSE program who allowed me to perform this wonderful journey in the field of Fire Safety Engineering. I personally want to thank Prof. Grunde Jomaas whose teaching brought me to the moral uplift and willing to strive for excellence.

I would like to appreciate the help of my supervisor Dr Cristian Maluk for the opportunity to perform the thesis at the University of Queensland, for help with organizing numerous aspects of my stay in Australia and for readiness to guide and help with any aspect of the present work.

I'd like to thank Prof. Luke Bisby for his guidance and advice.

Also, I want to thank Yunpeng Zhu for his practical help and scientific discussion of the problem.

The strongest *Thank You* goes to the whole team of Structures Lab of the University of Queensland, namely Chris Russ for helping with proper development and the assembly of the MTS actuator set-up, Fraser Reid for helping to organize my work, Ruth Donohoe for helping to keep everybody safe, Shane Walker for general guidance and helping with the plasterboard works, Stewart Matthews for being very practical and helping with making everything work and Jason Van Der Gevel for helping to fix the grounding machine.

Also, I'm very grateful to Van Thuan Nguyen and Mateo Gutierrez Gonzalez for helping with strain gauges and operating the 1 MN MTS actuator.

I want to thank Jeronimo Carrascal Tirado for providing all the assistance needed with the Fire Lab equipment.

I'm very grateful to my classmates who always helped to keep my spirit up and personally our best student representative Farah Faudzi who always guarded our interests and made our study process smooth.

I want to thank my wife Nastya for her infinite care and support throughout these 2 years of study. I couldn't have done it without you.

Lastly, I want to thank all of my family members who have been caring people giving their support and advice when needed.

CONTENTS

LIST OF FIGURES

LIST OF TABLES

NOTATION

c_p	thermal capacity
g	acceleration of gravity
h	height of a compartment
h_c	convective heat transfer coefficient
h_{eq}	weighted average of window heights on all walls
k_{air}	thermal conductivity of air
l	length of a compartment
L	length of the unexposed face of a specimen
m_{dry}	mass of a cubic sample after drying in an oven
m_n	mass of the cubic sample at normal conditions
$\overline{Nu}_L$	Nusselt number
O	opening factor
Pr	Prandtl number
$\dot{q}''_{conv}$	convective heat flux
$q_{f,d}$	fire load density
$\dot{q}''_{inc}$	incident heat flux
$\dot{q}''_{net}$	net heat flux to the concrete specimen
$\dot{q}''_{rad}$	radiative heat flux
Ra_L	Reyleigh number
Δt	timestep
t_{lim}	time limit of a fire growth phase
T_g	temperature of hot gases in a furnace
T_f	film temperature
T_j^i	temperature of concrete at the node *j* in the timestamp *i*
T_s	surface temperature of a concrete specimen
w	width of a compartment
Δx	size of a layer
α_{air}	thermal diffusivity of air

β_{air}	volumetric thermal expansion coefficient of air
ε	emissivity
θ	temperature of concrete
λ	thermal conductivity
ρ	density
σ	Stefan–Boltzmann constant
v_{air}	kinematic viscosity of air

This page is intentionally left blank

CHAPTER 1. INTRODUCTION AND OBJECTIVES

A fire in a building structure or any other infrastructure, such as a tunnel, is considered as a major hazard in modern fire safety design. Moreover, the amount of fire incidents in buildings and tunnels increases from year to year, causing structural damage, injuries and casualties (Casey, 2017) (Ren, et al., 2019). Also, fires involving vehicles and fires in buildings take more than half of the whole quantity of registered fires taking 15.9% and 37.3%, respectively (CTIF Center of Fire Statistics, 2019).

Concrete in comparison with other materials has historically been perceived as a 'safe' solution for achieving adequate structural response to fire due to its relatively low thermal diffusivity and non-combustibility. Concrete is a widely used construction material because of its wide availability, excellent mechanical properties and relatively low cost. Apart from that, it shows beneficial thermal properties, such as low thermal conductivity, which allows maintaining the acceptable temperature of the reinforcement for a relatively long time of a fire exposure without additional insulation.

However, with the improvement of high-performance concrete, the occurrence of explosive spalling became a limiting factor in the further development of high rise buildings and tunnels (Yang & Peng, 2010) (Hedayati, et al., 2015) (Mendis, et al., 2014). It was shown that high strength concrete (HSC) is more prone to spalling than normal strength concrete (NSC) due to lower permeability (Maraveas & Vrakas, 2014) (Maluk, 2014). Moreover, concrete spalling is often the main reason for structural collapse (Novak & Kohoutkova, 2018). This is the case when a significant amount of concrete cover spalls leaving the reinforcement exposed to hazardous heating from fire, which leads to fast degradation of mechanical properties of steel (Bailey, 2002). Also, the loss of concrete cross-section during a fire event leads to significant instantaneous reduction of compressive load-bearing capacity and stiffness of a column, precast concrete lining element or any other concrete structure. Apart from that, spalling may have progressive behaviour during a continuous fire leading to even higher losses (Phan, et al., 2011).

The historical precedent of tunnel and some building fires showed that damage caused by spalling results not only in high repair cost but also in financial losses from traffic re-routing, secondary structures damage, possible affected buildings and infrastructure above

the tunnel etc (Breunese, et al., 2008). Fire conditions in tunnels are often more severe in comparison with compartment fires in buildings based on different fuel involved, ventilation conditions, tunnel linings, geometry etc. Further development of infrastructure projects and the increase of vehicles with a large variety of goods which constantly diversifies put a demand on the structural response of structures in case of fire. Many historic tunnel fires such as Mont Blanc Tunnel (France) or St. Gotthard Tunnel (Switzerland) fires, turned into disasters, while the occurrence of a severe fire was thought of in a design stage. This shows that the assessment of the maximum possible reduction of damage to concrete structures caused by a fire is of the highest importance.

Maintaining the structural integrity, insulation and load-bearing capacity is dictated by building codes such as Approved Document B (Building Regulation 2010, 2013) in the UK or Building Code of Australia (BCA) (AS 3600:2018,). In the view of such fundamental requirements the techniques of mitigation of the occurrence of concrete spalling, a study of the influencing factors and conditions is an important research topic for concrete and construction industries.

1.1 Mechanisms of concrete spalling

Concrete spalling is a type of damage or destruction of concrete structures which leads to detachment of material from the exposed to heat flux concrete surface. It is referred to an instantaneous event of dislodgement of concrete pieces due to thermal instability (Hedayati, et al., 2015). Eurocode (BS EN 1992-1-2:2004,) distinguishes two types of spalling: explosive spalling and falling off of concrete in the cooling phase of a fire. The former one is tied with moisture expansion in the matrix of concrete and is characterized by a sudden and abrupt dislodgement of the material. The falling off concrete occurs at later stages of fire and refers to the cooling phase of a fire. During that stage inert chemical and mechanical processes of degradation of concrete properties are still ongoing while the influence of a fire is negligible.

Taking into account the non-uniform composition of the concrete body, casting and storing conditions, concrete spalling may occur in random points of the exposed surface. Thus, the reduction of the concrete cross-section of structural elements due to the spalling and a sharp increase in temperature deeper in the solid and near the reinforcement imposes hazard on the performance of structural members. Not only the degradation of steel and

concrete strength is driven by thermal processes, but also the bond contact between them. It makes concrete spalling a big issue in the development of the industry of concrete structures.

There are three mechanisms of spalling which are currently distinguished and discussed in the literature: thermo-hygral, thermo-mechanical and thermo-chemical (Liu, et al., 2018). Often, spalling is presented by a combination of several mechanisms which makes it a complex phenomenon. All of the mechanisms occur at different ranges of temperatures and require different measures for mitigation of concrete spalling.

The casted and cured concrete contains up to 7% of water moisture depending on the curing conditions and humidity in the surrounding air. Currently, four different types of pore water in cement paste are distinguished: C-S-H interlayer water, water in gel pores, interhydrate and capillary pore water (Wyrzykowski, et al., 2017). During heating, the expanding moisture tends to migrate deeper into the concrete body where the temperature is lower due to the thermal gradient. Following this process, a "moisture clog" is formed which blocks water from migrating further. Then, **thermo-hygral** or thermo-hydraulic concrete spalling is driven by the increase of pore pressure in the concrete body due to thermal expansion of chemically-bound and gel water (Fig. 1b). When the growing pressure exceeds the tensile strength of concrete, the spalling occurs. This mechanism is dominating in the range of temperatures at the spalled region from 220°C to 320°C (Liu, et al., 2018) (Ma, et al., 2015). Since thermo-hygral mechanism is tightly bound with concrete permeability, which allows moisture to migrate without increasing the pore pressure to extreme levels, such mechanism of concrete spalling is dominant in high strength concrete which has lower permeability if compared with normal strength concrete.

However, it is important to say that moisture content is not solely the property of concrete which defines the propensity to spalling by thermo-hygral mechanism. In the process of ageing of concrete the course of hydration is ongoing. It means that the moisture in pores of concrete is reacting with cement producing hydration products which narrow down and block the pores and microchannels. It is clear that such process leads to decrease of porosity of concrete.

On the other hand, upon drying and, consequently, shrinking of concrete microcracks are produced which connect the pores of concrete making a network which helps to transfer

water. Also, the process of escape of vapours leads to the creation of microchannels. These processes lead to the increase of the porosity of concrete.

Hence, to study the susceptibility of concrete to spalling by the thermo-hygral mechanism, a property which accounts both for concrete porosity and moisture content should be used. Such property is the degree of pore saturation (DPS) which decreases in the process of concrete ageing (Liu, et al., 2018).

When a concrete structure is exposed to heat, the thermal gradient is developed throughout the body imposing thermal stresses to be formed. Due to that, at some point, the complex stress-strain state is such that the developing tensile stress facilitates the occurrence of vertical cracks, which relieve the flaking of the concrete layer near the surface exposed to heat. Apart from large scale processes, the disproportion of thermal expansion between the aggregate and surrounding cement paste also takes place. This disproportion depends on the mix parameters and causes the increase of internal stresses in the concrete body. Such mechanisms of destruction are known as **thermo-mechanical** spalling (Fig. 1a). It is also tied up with the level of external loading and usually occurs at temperatures from 430°C to 660°C (Ozawa, et al., 2012) (Liu, et al., 2018).

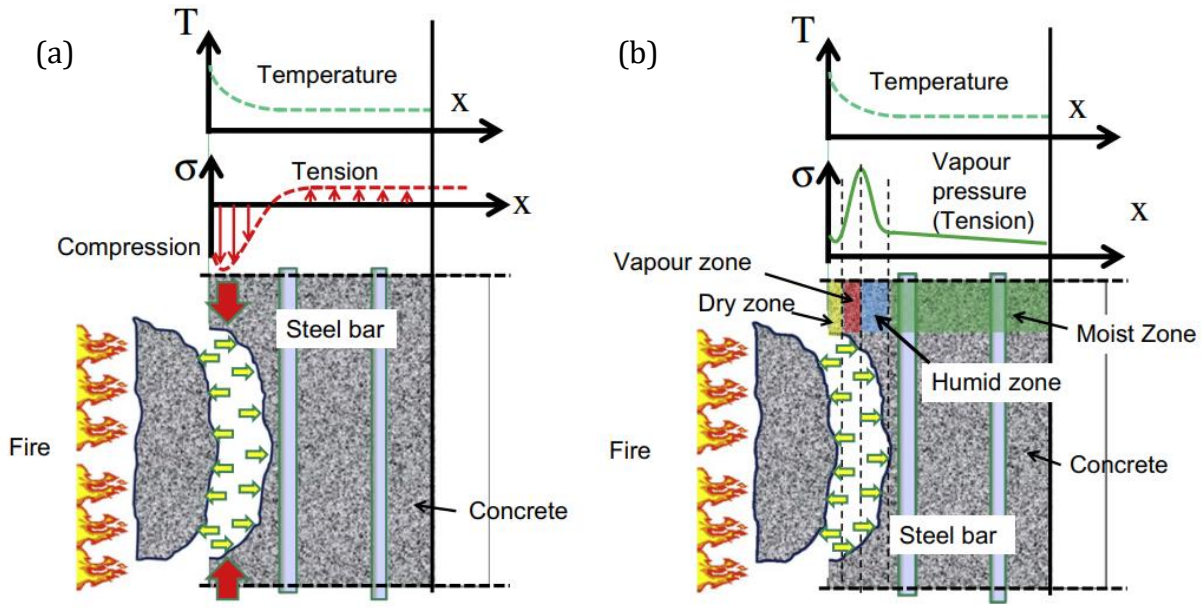

Figure 1. Diagrams of mechanisms of concrete spalling: thermo-mechanical (a) and thermos-hygral (b) (Ozawa, et al., 2012)

The main characteristic of thermo-mechanical spalling mechanism is the development of a stress gradient in the body of concrete. Another circumstance that can influence the development of such gradient is the internal stresses from boundary restraints and/or external loading. So, apart from heating conditions, the dominance of the mechanism is very sensible to the type of a structure, its service conditions and applied loads. Also, the presence of reinforcement plays an important role here, as it takes the tensile stresses thus obstructing the spalling concrete in that region of the concrete body.

Thermo-chemical type of spalling refers to the effect of chemical decomposition and degradation of properties of concrete and its' components at high temperatures. In particular, the reaction of decarbonisation of calcium carbonate is the main cause of spalling which takes place at temperatures higher than 700°C. Also, the effect of absorption of moisture from the atmosphere by newly formed calcium oxide from the dihydroxylation of the portlandite in cooling phase of fire exposure and its' subsequent significant expansion is distinguished as post-cooling thermo-chemical concrete spalling (Liu, et al., 2018) (Maluk, 2014).

It should be noted, that there is no clear agreement on the location of measurement of the mentioned temperatures. Also, it is known that the domination of a particular spalling mechanism is not only defined by a particular absolute temperature, but mainly by the temperature gradient, which varies with the rate of heating. In the research by Zhao et. al. (Zhao, et al., 2017) numerical analysis of concrete samples was performed and it was concluded that for slow heating regimes the thermo-hygral mechanism is dominating while for fast heating rate thermo-mechanical spalling governs the process.

Also, the strength of concrete plays a significant role in the definition of the dominating mechanism. Thus, as it is shown in the research by Gawin et. al. (Gawin, et al., 2018), normal strength concrete (NSC) is more subjected to thermo-mechanical spalling while for the high strength concrete (HSC) the thermo-hygral mechanism is the reported governing mechanism. Apart from that, those two mechanisms are considered to have similar contribution under slow heating of "relatively tight concretes". The active research on the dominance of each spalling mechanism in particular conditions is still ongoing, but the fact is that both thermo-mechanical and thermo-hygral mechanisms should be considered by researchers.

1.2 Influencing factors

The occurrence of concrete spalling was found to be influenced by a large variety of factors, which can be theoretically divided into 3 categories: properties of concrete mix, specimen conditions and conditions of heating. The influencing factors were studied by different researchers at different times and are summarized in Table 1 (Wang, et al., 2013) (Jansson & Boström, 2013) (Li, et al., 2019) (Memon, et al., 2019) (Missemer, et al., 2019) (Choe, et al., 2019) (Maluk, 2014) (Liu, et al., 2018).

Table 1. Factors affecting the occurrence of concrete spalling

Properties of concrete mix	Specimen conditions	Conditions of heating
• Aggregate type (calcareous, siliceous) and its grading; • Inclusion of air entrainment agents; • Water-to-cement ratio; • Permeability (porosity, tortuosity and connectivity of pores); • Inclusion of PP fibres (cross-section type (circular, rectangular) and size, length, dose, type (fibrillated, monofilament, multifilament), manufacturer); • Inclusion of steel fibres; • Other fibres (polyvinyl alcohol, cellulose, nylon, jute, raw rice husk); • Inclusion of silica fume; • Inclusion of fly ash; • Inclusion of superplasticizers; • Cement type and content.	• Moisture content; • Compressive strength; • Specimen type and shape, size; • Age; • Reinforcement type, ratio, location (cover), tie configuration; • Loading conditions (axial, bi-axial); • Mechanical restraints; • Curing conditions; • Casting technique.	• Heating set-up (furnace, H-TRIS, blowtorch); • Temperature-time curve; • Mode of heating (one face, multi-faced).

The list is not complete and is constantly updated according to contemporary research, development of new concrete mixes and testing techniques. Every listed parameter has a certain influence on the occurrence of concrete spalling. However, the influence of a combination of parameters is often unknown due to the limited amount of testing. This makes the effect of concrete spalling a complex problem and requires a fundamental understanding of concrete microstructure, its reaction to heat and how external actions influence those processes to develop adequate techniques of mitigation.

1.3 Methods of control and reduction of the likelihood of spalling

There is a certain agreement among researchers and scientists that the inclusion of polypropylene fibres in the concrete mix reduces the amount and the severity of spalling of concrete exposed to fire conditions (Bilodeau, et al., 2004) (Khoury, 2008).

Eurocode (BS EN 1992-1-2:2004,) provides 4 methods of prevention and mitigation of concrete spalling:

- Introduction of a reinforcement mesh with a nominal cover of 15 mm.
- Using a concrete mix which proved to be resistant to spalling.
- Insulation of potentially exposed faces of a structure.
- Inclusion of 2 kg/m^3 of monofilament propylene fibres.

Australian Building Codes (AS 3600:2018,) recommends the dosage of 1.2 kg/m^3 of 6 mm monofilament polypropylene fibres. Another common method of avoiding the loss of structural stability and integrity is the introduction of a so-called sacrificial layer of concrete, which is not effectively accounted in structural analysis as a loadbearing layer. However, standard methods of protection of concrete against the occurrence of spalling do not address the influencing factors and depend on the dominating mechanism of the effect (Mendis, et al., 2014). The most common way to reduce the probability of thermo-hygral spalling is to increase the permeability and to subsequently decrease the pore pressure of concrete by inclusion of polypropylene fibres which melt at ~165 °C leaving micro canals and thus reducing the pore pressure (Liu, et al., 2018) (Novak & Kohoutkova, 2018). However, as it was noticed in the research by Li et. al., the beneficial function of polypropylene fibres against concrete spalling is activated well below the melting point at temperatures above 125°C, which is the onset of melting of fibres (Li, et al., 2018).

Thermo-mechanical spalling can be decreased by the usage of calcareous aggregate instead of siliceous, adjusting the compression load level or inclusion of steel fibres in the concrete mix to reduce its brittleness (Liu, et al., 2018) It should be noted, that some load levels can be beneficial for the mitigation of concrete spalling effect. The research by Kim et. al. (Kim, et al., 2011) showed that load levels from 20% to 40% of the compressive strength of concrete can reduce concrete spalling due to increased permeability by means of micro-cracking. However, this refers mostly to thermo-hygral mechanism.

To reduce the thermo-chemical spalling of concrete it is advised to eliminate the usage of calcareous aggregate and lower the amount of cement in the mix (Liu, et al., 2018). As it can be seen, those methods are extremely restrictive leading to limitations in concrete strength and optimal mix design. On the other hand, the thermo-chemical spalling occurs only at high temperatures, starting from $700°C$ when the decarbonisation of calcium carbonate takes place.

Despite the fact that mechanisms are theoretically distinguished as involving different processes, they take place together in conjunction with each other. Some of the spalling reduction techniques for different mechanisms contradict each other, such as calcareous aggregate is more acceptable to mitigate thermo-mechanical spalling while should be avoided to reduce the probability of thermo-chemical spalling. Hence, complex mitigation techniques are required and the engineering approach should be taken to introduce adequate mitigation measures for the structural response to fire.

1.4 Influence of compressive loading

Generally, all concrete structures in the real world such as precast concrete tunnel segments, columns or walls are at the particular stress-strain state under working loading conditions and the testing should try to represent such conditions. For example, the level of loading of a concrete column or wall will depend on the imposed loads at the moment of fire and their joints' restraints. The compressive stress as a result of external loading or restraint conditions is viewed not only as a contributing, but also as a predominant factor to the propensity of concrete spalling (Maluk, 2014) (Deeny, et al., 2008) (Khoury & Anderberg, 2000) (Tanibe, et al., 2014) (Rickard, et al., 2016) (Rickard, et al., 2017).

Experimental research was carried out by Rickard et. al. (Rickard, et al., 2017) on concrete specimens with the cylinder strength of 48 MPa under compressive loading which were exposed to heating using H-TRIS apparatus which followed the modified Hydrocarbon (HCM) tunnel fire heating curve. The compressive stress due to loading appeared to be from 0% to 31% of the compressive strength of concrete and the spalling effect was likely to occur on specimens subjected to load levels of 21% and 31%. However, one specimen is reported to undergo spalling under 10% loading level. Authors concluded that compressive loading can dramatically change the spalling performance of concrete. However, there was no clear dependence of the severity of spalling from the load level found.

An experimental study of concrete specimens under loading conditions exposed to heating was performed by Kim et. al. (Kim, et al., 2011). Concrete with the strength of 24 MPa was tested using the HCM curve and load levels of 0%, 20%%, 40%, 60% and 70% of the compressive strength. The occurrence of spalling was observed in unloaded conditions but didn't occur at load levels of 20-40% of concrete strength because of "the smooth flow of vapours enabled by micro cracks". Similar results were received by Phan et. al (Phan & Carino, January-February 2002), who concluded that specimens stressed to the level of 40% of concrete strength led to the reduction of spalling.

Arita et. al. (Arita, et al., 2002) came to the conclusion that certain load levels decrease the severity of spalling. The experimental research was performed on 30 MPa and 108 MPa specimens subjected to ISO 834 heating curve in a furnace. The axial load levels were reported to be 0%, 10% and 33% of concrete's compressive strength.

In the research by Carré et. al. (Carré, et al., 2013) concrete slabs were exposed to heating under the compressive loading at levels from 0%, 13.5%, 27% and 40% of the compressive strength of concrete which constituted 37 MPa. The heating of the specimens was performed in accordance with ISO 834-1 fire curve using a furnace with 8 gas burners and lasted for 2 hours. The stress-strain state after the application of the load was assessed by means of strain gauges, glued to the exposed and unexposed surfaces of a specimen. The spalling effect was only observed on the load level of 40%. Authors conclude that there is an inverse relationship between maximum pore pressure and compressive stress from the applied load. This might be explained by the rise of concrete's permeability with compressive stress due

to the facilitation of microcracking. Apart from that, there is a conclusion that there is no clear correlation between maximum pore pressure in concrete and the spalling effect.

Extensive experimental research was recently performed by RISE - Research Institutes of Sweden in Borås (Boström, et al., 2018). Several intermediate-scale tests were performed and a comparison with full-scale tests was done subsequently. The most valuable findings of the research campaign were the definition of the most representative shapes and restraint conditions of specimens for the real-life behaviour of concrete. Thus, medium-sized (600 mm diameter and 300 mm depth) circular specimens moulded in steel rings showed the best correlation of the results of spalling testing in comparison with full-scale loaded reinforced concrete plates. Such specimen configuration is beneficial for the elimination of moisture evaporation from side edges by means of the steel ring. The ring also represents a restraint function putting a specimen in similar conditions to a locally heated region of a bigger concrete structure. Authors also concluded that compressive loading as well as faster heating conditions usually pose a higher risk of spalling.

Buch et. al. (Buch & Kumar Sharma, 2019) conducted experimental research on eccentrically loaded reinforced concrete columns subjected to ISO-834 fire curve in a modified furnace, which allowed the application of load. There were two types of concrete used for the fabrication of specimens: normal strength concrete of ~27 MPa and high strength concrete of ~62 MPa. The applied load constituted 33% of the ultimate axial design capacity of the column, however, the eccentricity of its application varied from 0 to 40 mm. Authors observed that more severe spalling occurred at the compressed face of the column than on the face subjected to tension due to eccentricity. It was concluded that eccentrically applied load facilitates the occurrence of concrete spalling. Moreover, normal strength concrete is more sensitive to eccentric loads in terms of spalling in comparison with high strength concrete.

A large research on the influence of the level of external loading on the occurrence of concrete spalling effect was conducted at the Politecnico di Milano, Italy, the Université de Pau et des Pays de l'Adour, SIAME, France, and the Centre Scientifique et Technique du Bâtiment (CSTB), France (Miah, et al., 2016) (Lo Monte, et al., 2019). The experimental testing of concrete specimens was performed with the application of uniaxial and biaxial

external loading. Specimens were cast using the concrete with the strength of ~50 MPa with two different types of cement. The heating conditions followed the ISO 834 curve.

Uniaxial loading was applied with a hydraulic jack which was fixed during the test, thus gradually increasing the load due to the thermal extension of specimens. The load levels were set to 0, 4, 8, 12, 16 and 20 MPa, constituting correspondingly 0%, 8%, 16%, 24%, 32% and 40% of the concrete's compressive strength under ambient conditions. The cubic specimens (200×200×200 mm) were exposed to heating at one face. The results showed the trend of increasing spalling behaviour with the increase of uniaxial loading.

The biaxial loading was performed using a specially manufactured steel frame with 8 hydraulic jacks. Specimens in the form of slabs (800×800×100 mm) were exposed to standard fire curve at one face. In that test different types of fibres were used to test the ability to mitigate concrete spalling under loaded conditions. Hence, monofilament and fibrillated polypropylene fibres, as well as steel fibres, were included in different mixes. In total there were specimens of each concrete mix. The cylindrical compressive strength of concrete at 288 days was reported to be ~60 MPa. The applied biaxial load constituted 10 MPa (17% of the concrete's compressive strength) and was maintained throughout the test to keep the compressive stresses constant. The results of the experiment showed the occurrence of spalling in both specimens without fibres and in the specimens with steel fibres.

Apart from the main part of the experiment, the authors compared the pore pressure which develops in concrete under 5 and 10 MPa biaxial compressive load. It was concluded that higher compression leads to higher damage to the hot layer such as microcracking followed my increased permeability which results in the reduction of pore pressure. This theory was used to explain higher values of measured pore pressure in specimens subjected to 5 MPa load in comparison with 10 MPa load.

The analysis of past research shows that that the maximum level of applied mechanical compressive loading was ~40% of concrete strength of HSC. Such value may be limited by the capacity of the equipment and experimental set-up. It can be concluded that the increase of compressive stress, in general, leads to more violent spalling. However, it was found that there is no clear dependence of pore pressure from the applied compressive loading. On the

opposite, it was shown that the permeability of concrete increases with the increase of compressive stress (Carré, et al., 2013).

The major quantity of research on concrete spalling is focused on the optimization of mix design, conducting experimental testing of specimen without loading conditions while controlling other parameters such as the dose of PP fibres, moisture content, different cement and aggregate types which leads to unrepresentative or deceptive results because a major spalling contribution factor is eliminated. Despite this fact, there is a number of scientists who in their research focus on the testing conditions such as external loading, restraints and relevant fire scenarios. It is clear that all of these aspects and some others do influence the occurrence of concrete spalling and only fundamental understating of the phenomenon, internal and external conditions of its occurrence may enable engineers to develop design techniques which will allow avoiding such negative effect in fire conditions.

1.5 Microcracking

A number of researchers claimed about the effect of microcracking which occurs either from rapid heating (Phan, 2008) or from applied loading (Carré, et al., 2013) (Kim, et al., 2011). The research by Wong et. al. (Wong, et al., 2009) showed a significant increase (in more than 2 times) in concrete permeability due to microcracking upon drying at the temperature of 105°C in comparison with 50°C. Also, temperature-induced microcracking is reported to occur at 150°C (Choinska, et al., 2007).

In the research by Li et. al. (Li, et al., 2018) the occurrence of microcracking is referred to the thermal expansion and mismatch between the larger aggregate and cement paste. Apart from that, it was found, that polypropylene fibres not only leave channels in the concrete body after melting, but they cause micro cracking due to thermal expansion of the fibres before melting. As the coefficient of thermal expansion of polypropylene is about 10 times bigger than concrete, it can cause significant tensile stress which may lead to the formation of microcracks (Fig. 2). The interconnected network of fibre channels and microcracks increases the permeability of concrete and helps to mitigate concrete spalling. Also, steel fibres are reported to facilitate the occurrence of microcracks (Li, et al., 2019).

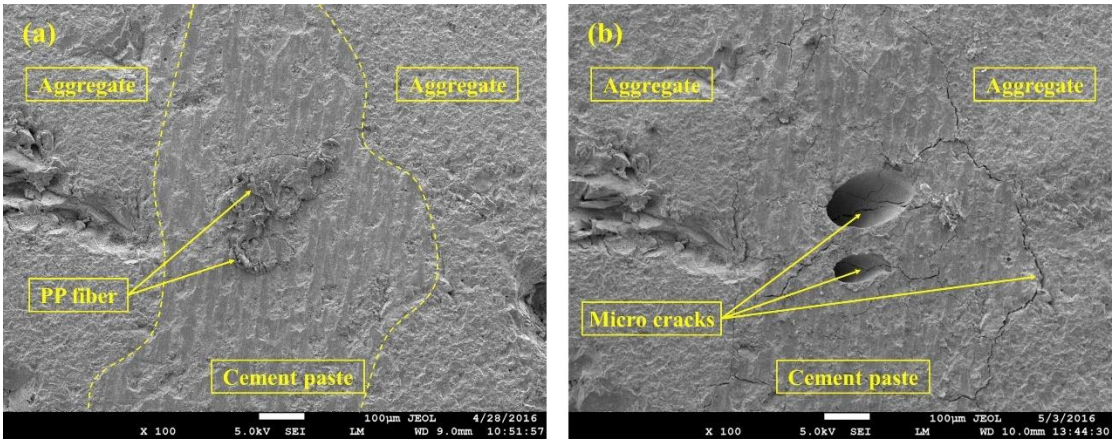

Figure 2. Microcracks caused by thermal expansion of polypropylene and thermal mismatch between the aggregate and cement paste. (a) before and (b) after exposure to 250°C (Li, et al., 2018).

The other reason for microcracking of concrete is the applied external load. In his studies, Loo (Loo, 1992) (Loo, 1995) concluded that the microcracking of concrete initiates at the axial compressive load levels between 15% and 40 % of concrete compressive strength. However, it was noted that the stress of the initiation of microcracking is very sensible to the type of structure and can statistically vary in a significant way. Also, it was noted that cracks do not propagate further until the load level of ~50%.

Other researchers refer to the constant or decreased permeability due to the closure of pores and microcracks during initial stages of loading. It is reported that at these stress level microcracks are mainly formed at the interfaces between aggregate and cement paste and they are not interconnected (Hoseini, et al., 2009).

1.6 Standard temperature-time curves

Most scientists use standard fire curves in their experimental research, which are: Hydrocarbon fire, Cellulosic fire, Parametric fires, Train or Car fires. Currently, the experimental knowledge of concrete spalling is mostly limited to those standard fire exposures. Despite the fact that those temperature-time curves do not represent a real fire and have only one period of temperature growth, they are still widely applied because of comparability and reproducibility of results. Also, the Eurocode provisions (BS EN 1992-1-2:2004,) considering spalling apply only for a standard temperature-time curve.

ISO 834 which is also called a Cellulosic fire refers to a compartment fire development with cellulosic fuel like wood and is usually used for testing of building materials and structures in furnaces to assign a certain fire rating or Fire Resistance Level (FRL). Apart from standard fire curves in performance-based approach, custom fire curves can be developed based on fire load, ventilation conditions, properties of compartment lining etc. Such custom curves are based on the procedures described in Eurocode (BS EN 1991-1-2:2002,) and are called parametric fire curves.

However, the standard curve does not represent the speed of fire growth in cases when liquid hydrocarbon fuels are involved. This is specifically relevant for tunnel fires where vehicles loaded with petrol, oil or chemicals may be involved. Apart from that, the experience shows that even non-hazardous materials and substances which have big calorific values involved in tunnel fires lead to disastrous consequences, such as margarine in Mont Blanc tunnel fire or tarpaulins and vehicle tyres in Gotthard road tunnel fire (Voeltzel & Dix, 2004). In this demand, a Hydrocarbon (HC) and Modified Hydrocarbon (HCM) were developed by French Ministry of Equipment (Ministère de l'Equipement, 2000) and are actively used to represent such severe tunnel fire conditions. These two curves have the same shape, but different peak temperature.

Another vision of how a nominal temperature-time fire curve for a tunnel should look like was released by German regulations (RABT 02, 2002) (ZTV - Tunnel, 1995, 1999) in two versions: a car and a train fire. Both curves rapidly achieve the peak temperature of 1200°C but unlike other curves have cooling phases: after 30 minutes for a car and after 60 minutes for a train.

With the progress in the research of the performance of concrete linings in tunnels and practical experience the RWS curve was developed in the Netherlands by Rijkswaterstaat (RWS) and Efectis (Breunese, et al., 2008) (Maraveas & Vrakas, 2014). The RWS curve shows similar to HCM temperature rise rate with a slightly higher peak temperature of 1350°C at 60 min and a subsequent gradual decrease to 1200 °C at 120 mins. Among other requirements, the mentioned RWS and Efectis testing procedure for concrete tunnel linings require the application of representative compression load. Apart from that, it allows aaplying an eccentric load to model the corresponding compressive stress on the exposed concrete surface.

All of the discussed nominal temperature-time curves are plotted in Fig. 3.

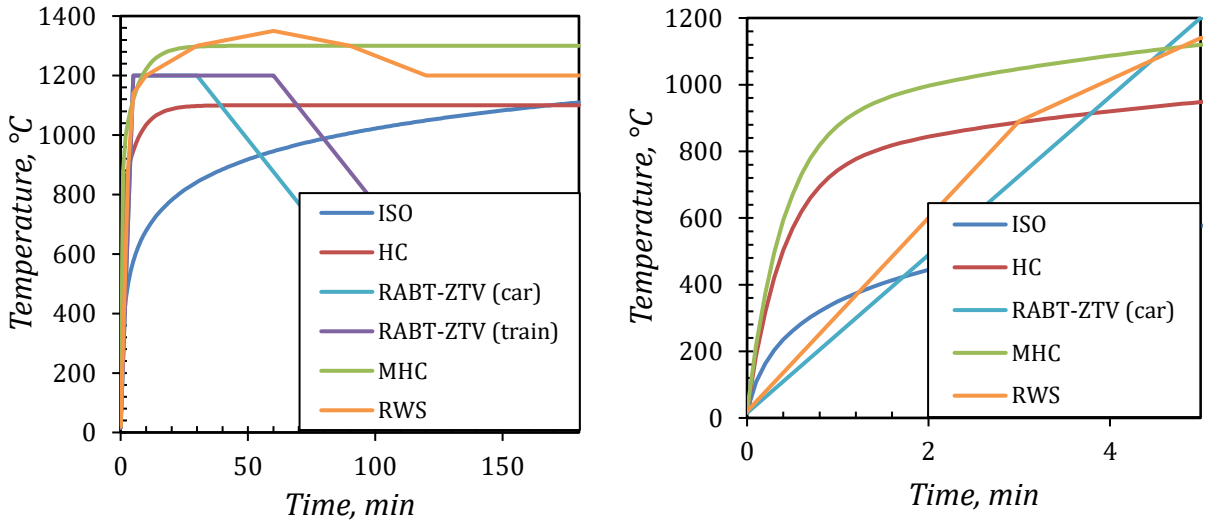

Figure 3. Most widely used nominal temperature-time curves

The analysis of the development of nominal fire curves shows that the aim of the historical improvements was to increase the maximum temperature in the initial stages of a fire, like MHC or RWS curves. However, it should be noted, that higher heating rates do not always lead to more severe spalling. For example, it was reported by Phan (Phan, 2008) that faster heating may result in lower pore pressure due to the development of microcracks and further to the mitigation of spalling.

1.7 Research objectives

Many scientists report that there is still a lack of experimental research on concrete spalling in loaded conditions, which potentially can be more applicable for the work of designers and fire safety engineers (Liu, et al., 2018). Also, the major part of testing with compressive load was held using the ISO 834 temperature-time curve, which does not represent the whole variety of heating conditions which are present in compartment and tunnel fires. The major part of the experimental testing discussed in previous sections had been done without any applied load, which eliminates an important influencing factor. Also, it distances from the real service conditions of a concrete structure. Although large efforts are made towards a fundamental understanding of the spalling phenomenon by means of scientific research, there is still no consensus among scientists on the influence of mechanical loading and heating conditions on the propensity of concrete to spalling.

The understanding of the heating conditions which may represent real fire scenarios together with realistic loading level is of higher importance due to the representation of closer-to-practice conditions.

The main goal of the present research is to define the influence of different levels of compressive loading conditions in combination with a range of parametric fire scenarios on the occurrence of the spalling effect in concrete with the inclusion or absence of polypropylene fibres in the mix. This research is also an important part in the understanding of the influence of the sustained compressive stress on the occurrence of spalling.

CHAPTER 2. METHOD

2.1 Experimental set-up

The aim if the experimental testing was to study the occurrence of the explosive concrete spalling under simultaneously applied mechanical compressive load and radiative heat. To achieve this, the two apparatuses were used: Heat-Transfer Rate Inducing System (H-TRIS) and 1 MN MTS hydraulic actuator (Fig. 4).

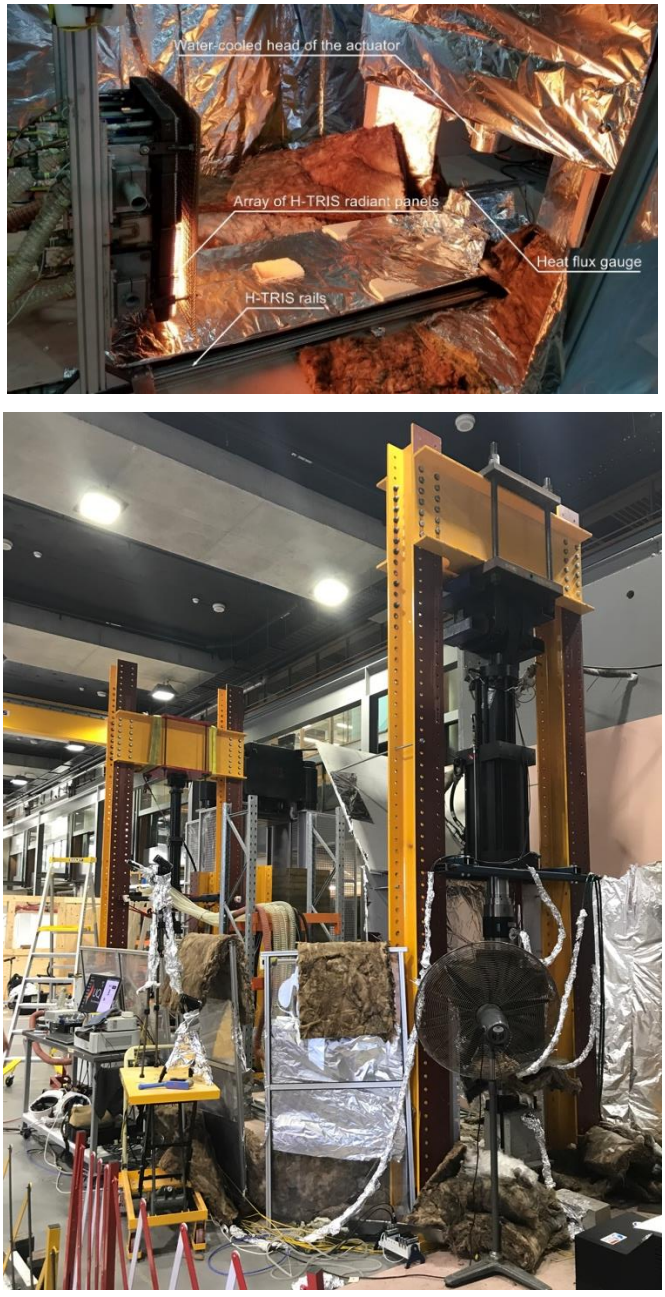

Figure 4. A general view of the experimental set-up during calibration

The rails of the H-TRIS apparatus were installed right in front of the plane of action of the actuator to achieve the maximum heat flux. All of the potentially affected equipment was covered with insulating materials.

2.1.1 Compressive loading

The compressive stress was applied by means of a 1 MN hydraulic MTS actuator, which was installed on a steel frame. The actuator head was protected from overheating by an in-built water-cooling system The whole mechanical set-up was protected with plasterboard and rockwool to eliminate technical faults due to heating. The force from the actuator was transferred on the upper face of the specimen eccentrically through a steel plate in order to distribute the pressure and to achieve the maximum compressive stress at the exposed surface (Fig. 5). Concrete samples were fixed on the steel base with the fixing plank and fixing details near the corners in order to keep them right in the same place in every test. This will help to achieve the maintenance of the same point of load application.

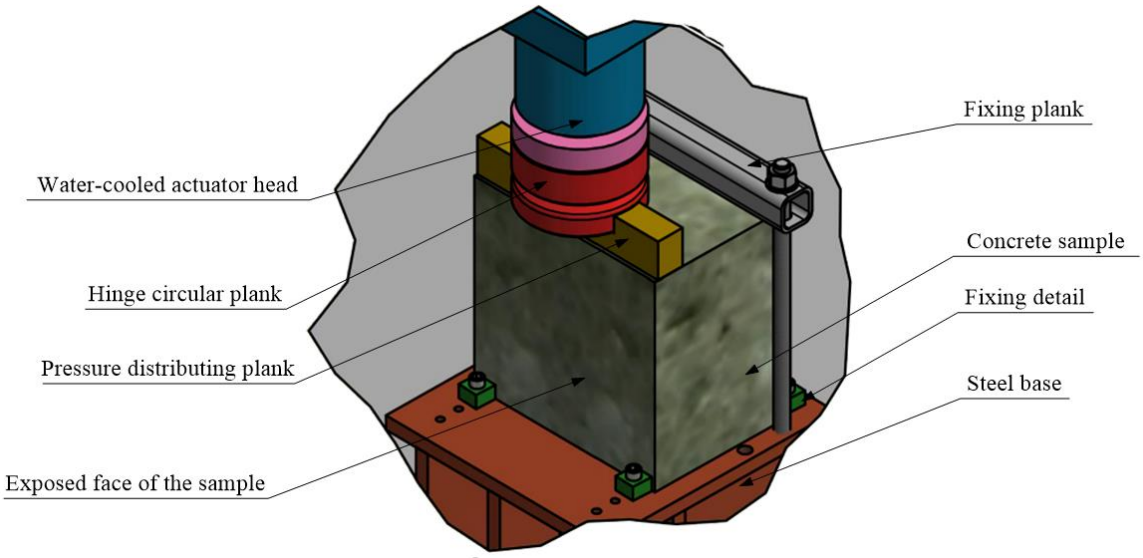

Figure 5. A 3D sketch of the mounting of a concrete specimen in the test set-up

The induced compressive strain at the exposed (front) surface was measured with the help of glued strain gauges (Fig. 6). The strain gauges with the measurement base of 60 mm were located on the centreline of the specimen. The glueing process involved the preparation of concrete surface with sandpaper with further treatment with Acetone, conditioner and neutraliser.

Despite the fact that the samples were equipped with strain gauges on the exposed surface, the level of sustained compressive loading was defined by the compressive force on the actuator. The magnitude of the compressive force constituted 160 kN, 280 kN and 400 kN. To maintain the consistency of the research the specimens were placed in the same location of the steel base and the point of the applied force was maintained invariably.

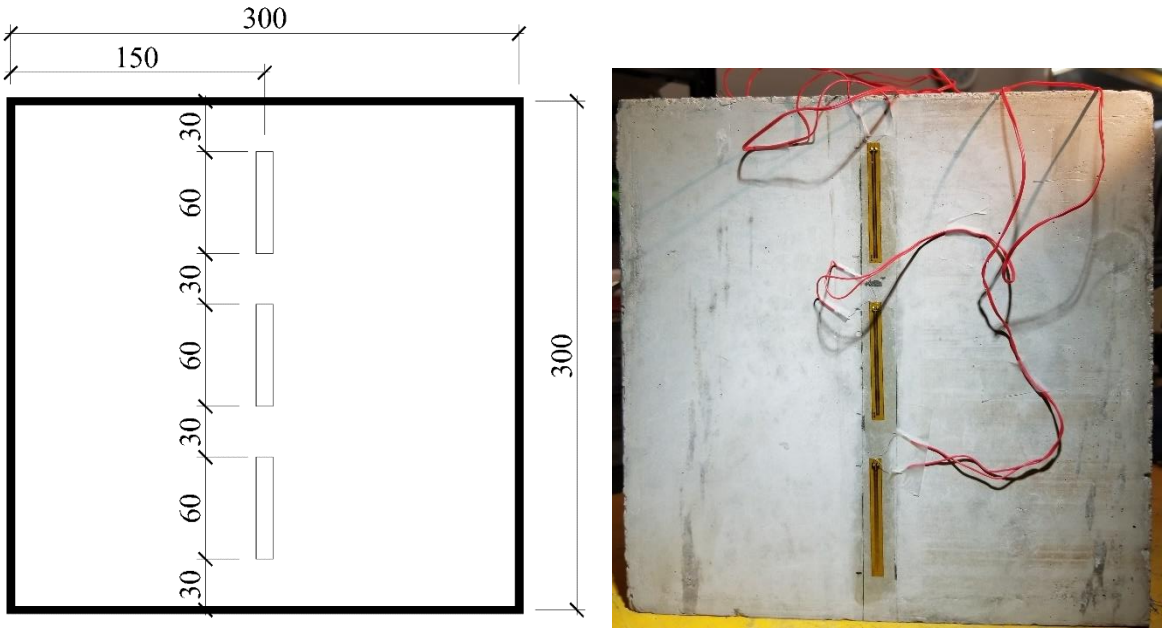

Figure 6. The diagram of the location and an actual view of strain gauges on the exposed surface of a concrete specimen

Initially, the load of 50 kN was applied and taken off in order to press all the components of the set-up and eliminate additional displacements during the main loading. After that, the compressive load was applied gradually, slowly incrementing the force and reaching the maximum pressure after ~3 minutes. The load was maintained for 5 minutes after which the values of strains were recorded.

While maintaining the compressive load on a chosen level, the front face of a specimen was exposed to an incident radiative heat flux by the H-TRIS apparatus.

Initially, the specimen was covered with a protective material while the radiant panels were heating up. After this, the experiment started with removing the protective material and thus exposing the surface to the incident heat flux. The programmable motor followed the programmed distance-time curve. The test lasted until a spalling event occurred or for

the maximum defined duration of 60 minutes. During the experiment, the exposed surface of a concrete specimen was in clear view which allowed to notice the occurrence of spalling instantaneously. Due to the fact that during the exposure to the incident heat flux the temperature of the exposed concrete surface quickly reaches the limits of the strain gauges range of operation temperatures, the strains were not controlled during the experiments.

2.1.2 H-TRIS apparatus

Historically, the compliance of structures to fire safe design was proved by conducting a standard furnace test, where temperature follows the defined curve, the first of which was established in 1917. This test does not represent the real fire conditions, however, imposing more severe heating in most cases. Due to that fact and other circumstances, it remains unchanged since introduction. The over 100-year advancement in fire science gained documented test results and real-fire experience, CFD modelling techniques led to the certain level of understanding of compartment and tunnel fires, their development stages and possible temperature-time and incident heat flux – time curves. Standard furnace test procedure usually does not allow to apply compressive load to a specimen or to control the heat flux to the exposed surface. However, scientists and researchers modify or design custom furnaces which meet the needs of an experiment.

Currently, there is no unified testing technique established to test the propensity of concrete to spalling (Boström, et al., 2018). The main parameters of experiments such as test set-up, heating conditions or specimen size are set arbitrarily by a client and an organization which performs the test. In general, full-scale tests are more expensive and very time-consuming. That is why the major part of the research is done in medium or small scales. Due to this circumstance, the produced results are often contradictory since full scale loaded specimen do spall significantly while small scale unloaded ones do now show any spalling at all. Moreover, there is no methodology of measurements which need to be made during an experiment. Often, the occurrence of spalling and an arbitrary assessment of the “severity” is reported, and the comparability of results is very low due to different specimen shapes, heating conditions and apparatuses, concrete mixes etc.

All these created a need in more sophisticated testing technique which may give certain freedom to a researcher to apply the thermal loading to a structure in terms of

programmable incident heat flux – time history curve and controlling thermal boundary conditions. In this demand, an H-TRIS (Heat-Transfer Rate Inducing System) apparatus was created. It enables the testing of medium-scale structures by applying the programmed incident heat flux – time history curve on the exposed surface of a specimen. Apart from that, the apparatus introduces high repeatability of experimental results, lowers the testing costs and provides a variety of possible thermal exposures. At the same time, H-TRIS remains the possibility to reproduce the temperature-time curves which are used in standard furnace testing.

The apparatus mainly consists of an array of radiant panels and a programmable motor which is capable of moving the panels back and forward thus varying the incident heat flux by changing the distance between the panels and the exposed surface of a specimen. The calibration process involved the measurements of incident heat flux at the whole range of distances between the radiant panels and the exposed surface of the concrete sample. As the result of completed calibration an incident heat flux – distance curve is created. After the calibration, the apparatus was programmed to follow the desired incident heat flux – time curve.

2.2 Heating conditions

Heating conditions for the experimental research were designed using parametric temperature-time curves according to the procedure described in Eurocode (BS EN 1991-1-2:2002,). The parametric curves include both heating and cooling phases and its shape is defined by a number of parameters:

- fuel load density in the assumption that it will be fully burnt out;
- an opening factor which depends on the area and height of openings;
- thermal properties of boundaries;
- parameters of an enclosure.

A compartment with concrete linings was assumed to create a number of scenarios involving the variable parameter of the opening factor. Thermal parameters of compartment boundaries were taken at ambient temperature. The parameters taken for that process are presented in Table 2.

Table 2. Selected parameters used to design parametric fire curves

Parameter	Symbol	Taken value
Properties of compartment boundaries		
Thermal conductivity	λ	*1.6 W/m·K*
Density	ρ	*2300 kg/m^3*
Thermal capacity	c_p	*980 J/kg·K*
Parameters of the fire		
Time limit of growth phase	t_{lim}	*0.25 h*
Fire load density	$q_{f,d}$	*511 MJ/m^2*
Dimensions of the compartment		
Width	w	*8.0 m*
Length	l	*19.5 m*
Height	h	*3.4 m*
Weighted average of window heights on all walls	h_{eq}	*1.7 m*

The abovementioned parameters remained constant for all of the parametric temperature-time curves. The variable parameter was the opening factor, which was calculated using the opening width and height dimensions, which are presented in Table 3.

Table 3. Dimensions of the openings used to calculate the opening factors of parametric fire curves

Dimension	O = 0.0415 m$^{1/2}$	O = 0.0515 m$^{1/2}$	O = 0.1 m$^{1/2}$	O = 0.2 m$^{1/2}$
Width of the opening	*7.316 m*	*9.1 m*	*17.645*	*35.39 m*
Height of the opening	*2 m*	*2 m*	*2 m*	*2 m*

The method of parametric fire curves described in Eurocode (BS EN 1991-1-2:2002,) has the following defined limitations:

- the opening factor O can vary from $0.02\ m^{1/2}$ up to $0.2\ m^{1/2}$;
- thermal absorptivity for the total enclosure ($b = \sqrt{\rho c \lambda}$) should be limited between $100\ J/m^2 s^{1/2} K$ and $2200\ J/m^2 s^{1/2} K$;
- compartment floor area should be no more than $500\ m^2$;
- the maximum ceiling height is $4\ m$.

The upper limit of the opening factor $O = 0.2\ m^{1/2}$ defined the "short-hot" parametric temperature-time curve for the assumed compartment. The designed curves were theoretically divided into "slow" heating curves with $O = 0.0415\ m^{1/2}$ and $O = 0.0515\ m^{1/2}$, and "fast" heating curves with $O = 0.1\ m^{1/2}$ and $O = 0.2\ m^{1/2}$. This division is arbitrary and is introduced for better communication with the reader. All four curves are presented in Fig. 7Figure 7.

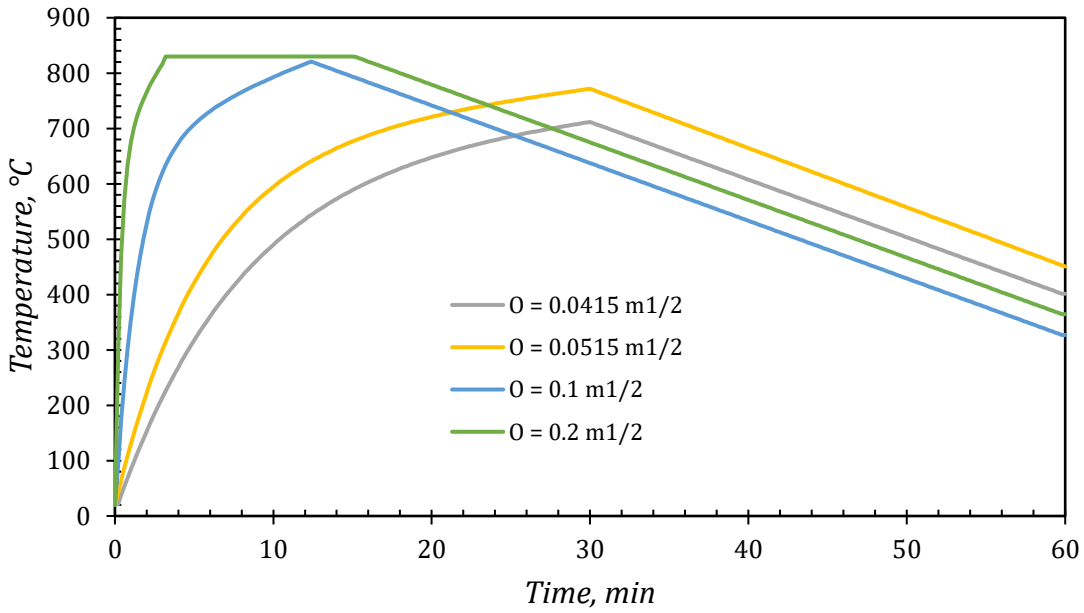

Figure 7. Designed parametric temperature-time curves

The flat region of the curve with $O = 0.2\ m^{1/2}$ is dictated by the limitations of the maximum incident heat flux of the H-TRIS apparatus in the designed set-up conditions. The curve with $O = 0.0515\ m^{1/2}$ was intentionally designed to match the timing of the growth phase of the curve with $O = 0.0415\ m^{1/2}$ for better comparability of the results.

Despite the fact that the designed parametric temperature-time curves were calculated for a compartment, the growth rate of "fast" fires turned out to be comparable to those of most common nominal tunnel fire curves. The comparison of the first 5 minutes of the tunnel fire curves with the designed parametric fire curves is presented in Fig. 8.

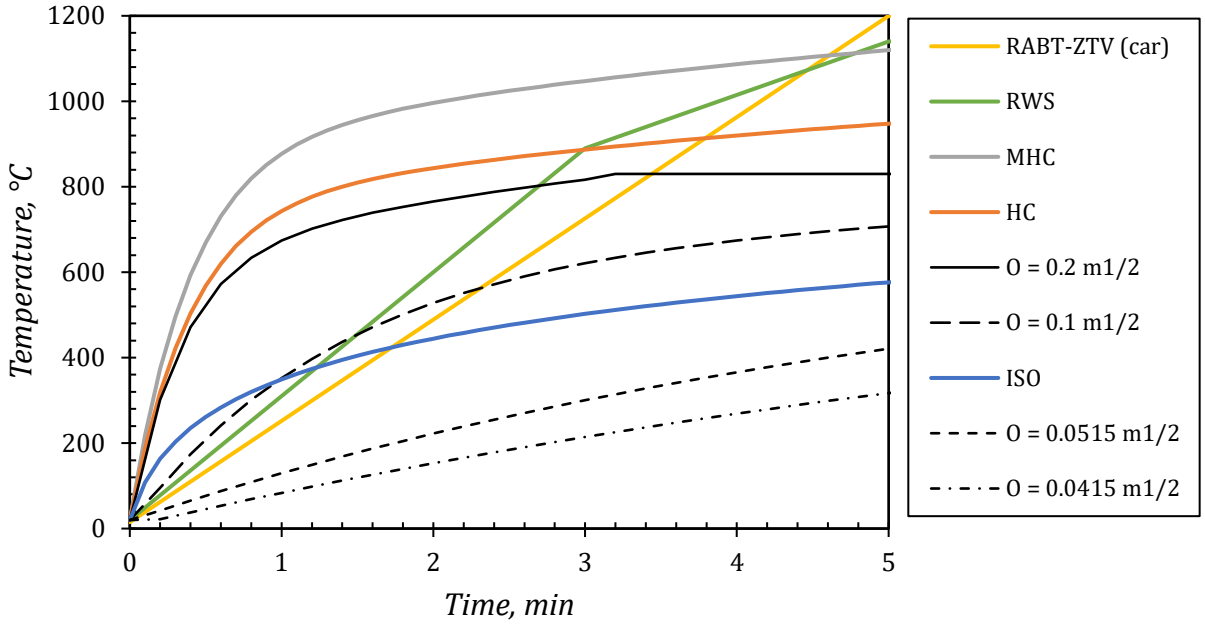

Figure 8. Comparison of the first 5 minutes of the most common temperature-time curves with the designed parametric curves

As it can be seen from the graph above, the parametric curve with $O = 0.2\ m^{1/2}$ has similar growth rate with the hydrocarbon curve and it higher heating rate than RWS or RABT-ZTV in the first 5 minutes of heating.

After the temperature-time curves were defined, they became the input parameters for the calculation of the incident heat flux – time curves using the finite difference method described in next chapters in order to recreate the thermal exposure which a sample experiences in a standard furnace testing. The calculated incident heat flux – time curves (Fig. 9) were further used in tests by means of H-TRIS apparatus.

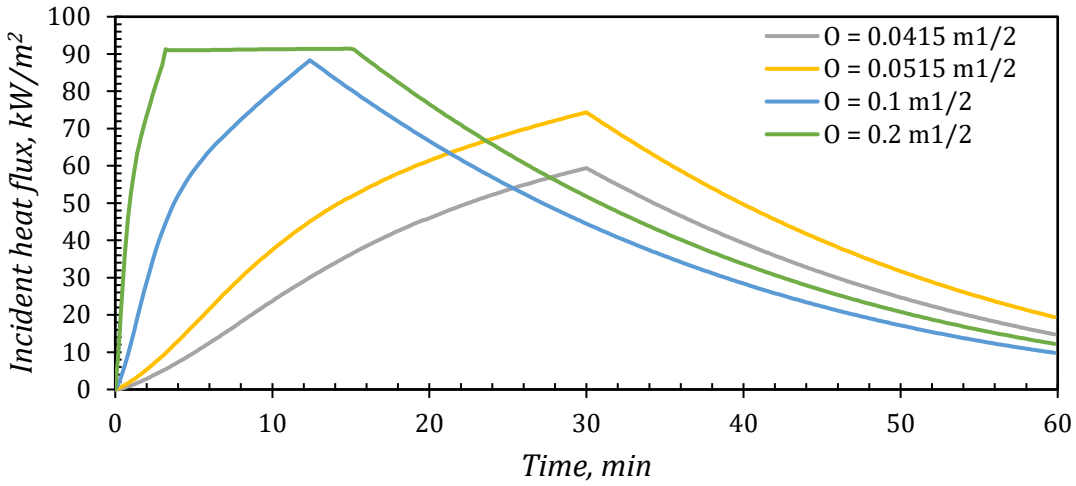

Figure 9. Incident heat flux-time curves for H-TRIS apparatus

One of the main parameters which show the thermal performance of a concrete specimen during testing is the amount of heat absorbed by its exposed surface. This value can be calculated by subtracting the convective and radiative losses from incident heat flux. Such convective and radiative losses occur due to the heating up of the specimen and they grow with the increase of the temperature. The graphs which represent the time history of heat flux absorbed by a concrete specimen are shown in Fig. 10.

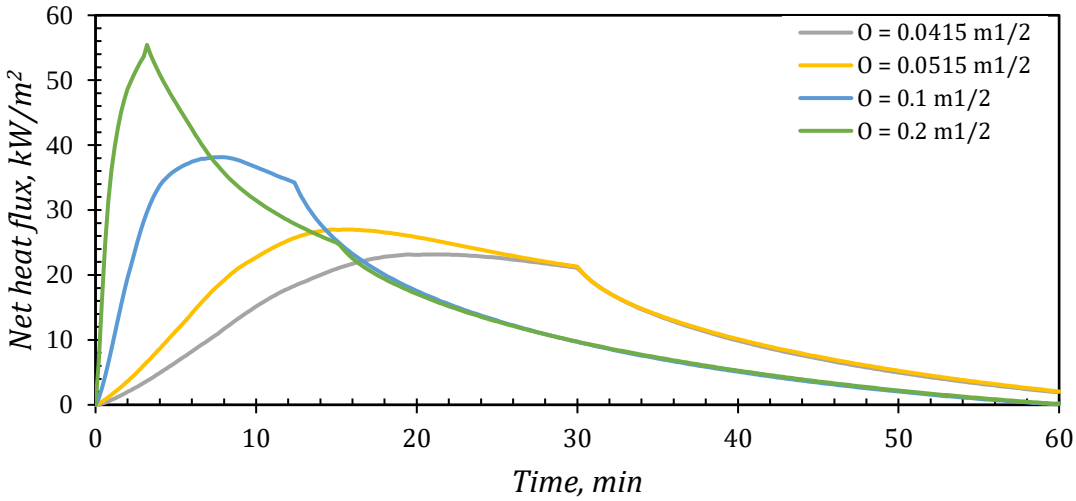

Figure 10. Net heat flux - time history of a concrete specimen exposed to fires which were designed with temperature-time parametric curves

2.3 Samples

In the described research concrete specimens with dimensions of 300×300×220 mm were cast in the laboratory of The University of Queensland. The composition of the concrete mix is presented in Table 4. One part of those specimens was earlier tested by Thorne (Thorne, 2018), another part was left for the current research.

Table 4. The composition of plain concrete used in the experiment

Mix Component	Quantity by Mass	Mix Component	Quantity by Mass
LWR – WRDA PN 30	533 ml	Fly ash	33 kg
Sand (Brendale)	171.3 kg	Imported Sand	187 kg
Cement GP	116.6 kg	Silica Fume	5 kg
Cryna 10 mm Aggregate	200 kg	Water	45 L

The samples were left in the framework for 24 hours after casting, covered with plastic sheets. After that, they were cured in water for 7 days at 20°C and then put into the room with controlled environment of 50% humidity and 23°C ambient temperature. The samples were kept under that conditions until testing.

Concrete specimens were cast with embedded thermocouples along their depths which allowed to measure the temperatures and to estimate temperature gradients during the exposure to radiative heat flux. The locations of thermocouples in concrete samples are summarized in Appendix A. The technique of fixing of thermocouples in the desired locations is based on the usage of plastic guide wires and is described in the work by Thorne (Thorne, 2018).

The amount of PP fibres used in the corresponding part of samples constituted 1.6 kg/m^3, which is an average value between the amount recommended in the Eurocode (BS EN 1992-1-2:2004,) and in Australia Building Code (AS 3600:2018,). Such amount of PP fibres was added to the matrix of the experimental research in order to study the significance of introducing the fibres in the concrete mix and its efficiency to mitigate the concrete spalling under compressive loading conditions The test matrix of the experimental research is presented in Table 5.

Table 5. Test matrix of the experimental research

Compressive loading	O = 0.0415 $m^{1/2}$	O = 0.0515 $m^{1/2}$	O = 0.1 $m^{1/2}$	O = 0.2 $m^{1/2}$
No load	No PP fibres	No PP fibres	—	—
19% 160 kN	No PP fibres	—	No PP fibres	—
40% 280 kN	No PP fibres	No PP fibres	No PP fibres 1.6 kg/m^3 PP	—
53% 400 kN	No PP fibres	—	1.6 kg/m^3 PP	1.6 kg/m^3 PP

The type of PP fibres used is Propex monofilament fibres with the length of 12 mm. Such type of fibres had been chosen because it showed a lower propensity to spalling (Maluk, et al., 2017).

The strength of concrete used in the experimental research was determined by means of compression tests of cylinders with standard dimensions 100×200 mm and constituted 55.67 MPa. The cylinders were cast on the same day and from the same concrete mix as the main block samples. The abovementioned cylinders were tested on the first day of the experimental research. The ultimate compressive strength was calculated as the average value of 3 tested samples. The test data is presented in Table 6.

Table 6. Test data of the determination of concrete strength

Sample number	Date of test	Age of concrete	Force of failure, kN	Strength, MPa
1	04/04/2019	309 days	412.3	52.5
2			452.2	57.58
3			447.1	56.93
			Average:	**55.67**

For the calculation of the ultimate vertical strain, the elastic modulus was taken from Eurocode (BS EN 1992-1-1:2004+A1:2014,) for the concrete class C55/67 which constituted 38 GPa.

The moisture content of concrete samples tested in the present research work was determined as a percentage of dry mass by a convection oven drying. Concrete cubes with dimensions 100×100×100 mm were cast from the same mixes on the same day with the main samples. The cubes were cured at the same conditions with block samples in the same room until the first day of the experimental research. These cubes were weighed and put in an oven at 105°C. The weight of cubes was checked occasionally until it changed less than 0.01% during 24 hours of drying. After that, the moisture content was calculated as:

$$MC(\%) = \frac{m_n - m_{dry}}{m_{dry}} \cdot 100\% \quad (1)$$

where m_n is the mass of the cubic sample at normal conditions, g;

m_{dry} is the mass of a cubic sample after drying in an oven, g.

The moisture content of the abovementioned cubes was determined in time of the experimental research. The results are presented in Table 7.

Table 7. Test data of the determination of concrete moisture content

Sample number	Period of drying	Age of concrete	Moisture content, %
1	16/04/2019 - 20/04/2019	309 days	3.5
2			3.9
3			3.4
		Average:	**3.7**

2.3.1 Labelling of samples

The samples in this experimental research were labelled in the following way: HC0.1_L40%_PP1.6. It can be divided into 3 parts: heating conditions, level of compressive loading and the amount of PP fibres included in the mix. In the example above the sample

with 1.6 kg/m^3 PP fibres in the mix was exposed to the loading which corresponds to the stress on the exposed surface which constitutes 40% of concrete compressive strength. The heating conditions followed the parametric temperature-time curve, which was calculated using the opening factor of *0.1 $m^{1/2}$.*

2.4 Heat transfer model

2.4.1 Heat absorbed by a specimen in the furnace

The main aim of the following modelling is to calculate the time history of the heat flux which is absorbed by a concrete specimen in a standard furnace test by radiation and convection in order to replicate it by means of the H-TRIS apparatus. This term is called the net heat flux and is calculated as a sum of radiative and convective heat fluxes from hot gases in a furnace:

$$\dot{q}''_{net} = \varepsilon\sigma\left(T_g^4 - T_s^4\right) + h_c\left(T_g - T_s\right) \quad (2)$$

where $\dot{q}''_{net}$ is the net heat flux to the concrete specimen, W/m^2;
ε is the emissivity of hot gases in the furnace;
σ is the Stefan–Boltzmann constant, 5.67×10^{-8} W/m^2K^4;
T_g is the temperature of hot gases in the furnace, K;
T_s is the surface temperature of a concrete specimen, K;
h_c is the convective heat transfer coefficient in the furnace, W/m^2K.

The calculation of the term in each timestep requires the finding of the surface temperature from the previous timestep as an input parameter. To find the surface temperature with known net heat flux, the temperature gradient in a concrete specimen is calculated using a finite difference method. This approach is based on the division of the concrete body into a number of layers with the length Δx and assigning a node in the centre of each layer (Drysdale, 2011) (Maluk, 2014) (Bergman, et al., 2016) (Fig. 11). The one-dimensional representation of the model was used to calculate the temperatures in each layer of a concrete specimen by means of transient heat transfer, which then were used in calculations of incident heat flux to reproduce it with H-TRIS apparatus. Apart from that,

calculated temperatures were later compared to measured values in concrete specimens by means of installed thermocouples.

The basic assumption of the model is that the body is infinite and the heating is uniform on all the surface. Only the exposed surface is considered to be receiving energy. Also, it was assumed that there is no other heat loss other than from the back of the concrete body.

The edge nodes are placed not in the centres of the edge layers with the lengths $\frac{\Delta x}{2}$ but on their borders. Then, the temperature inside the body is calculated at each node based on conduction between the adjacent nodes with different temperatures. At the node at the exposed surface, the $\dot{q}''_{net}$ is used to put energy into the model. At the last node of the model, which represents the back (unexposed) face of a concrete specimen, when it is heated by an adjacent layer, the convective and radiative losses remove energy from the model.

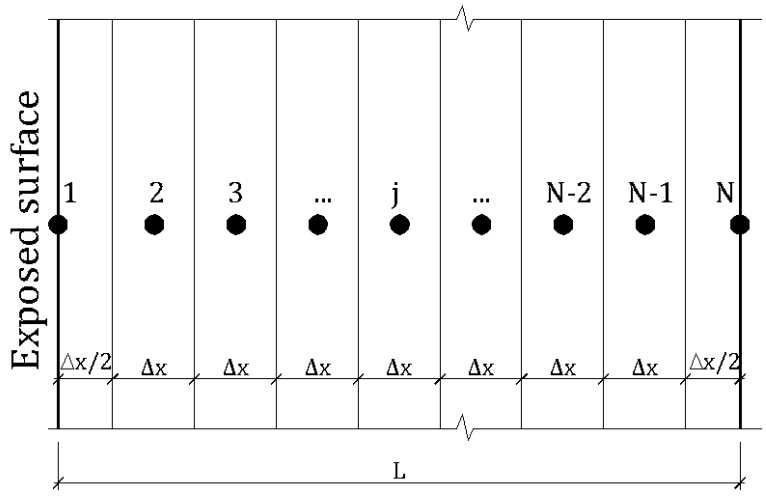

Figure 11. Division of a concrete specimen into a number of layers.

The temperature in the first node (exposed surface) is governed by the net heat flux from the hot gases in a standard furnace and further conduction to the second node. It can be found as:

$$T_1^{i+1} = T_1^i + \frac{2 \cdot \Delta t}{(\rho c)_1^i \cdot \Delta x} \cdot \left[\dot{q}''^{\,i}_{net} - \left(\frac{\lambda_1^i + \lambda_2^i}{2} \right) \cdot \left(\frac{T_1^i - T_2^i}{\Delta x} \right) \right] \quad (3)$$

where T_1^{i+1} is the temperature of concrete at the node of the exposed surface in the subsequent timestep, *K;*

T_1^i is the temperature of concrete at the node of the exposed surface in the present timestep, *K*;

Δt is the timestep, *s*;

ρ is the density of concrete at present temperature, kg/m^3;

c is the specific heat of concrete at present temperature, *J/kg K*;

Δx is the size of a layer, *m*;

$\lambda_{1,2}^i$ is the thermal conductivity of concrete at nodes 1 and 2 at present temperature, *W/m K.*

The temperature in an inner node *j* is described by the conduction with the adjacent nodes:

$$T_j^{i+1} = T_j^i + \frac{\Delta t}{(\rho c)_j^i \cdot \Delta x^2} \cdot \left[\left(\frac{\lambda_{j-1}^i + \lambda_j^i}{2} \right) \cdot \left(T_{j-1}^i - T_j^i \right) - \left(\frac{\lambda_j^i + \lambda_{j+1}^i}{2} \right) \cdot \left(T_j^i - T_{j+1}^i \right) \right] \qquad (4)$$

where T_j^{i+1} is the temperature of concrete at the node *j* in the subsequent timestep, *K;*

$T_{j-1,j,j+1}^i$ is the temperature of concrete at the nodes *j-1, j* and *j+1* in the present timestep, *K*;

$\lambda_{j-1,j,j+1}^i$ is the thermal conductivity of concrete at nodes *j-1, j* and *j+1* at present temperature, *W/mK.*

The temperature in the node N which represents the unexposed face is based on the conduction heat transfer from the adjacent node N-1 and further dissipation of heat by radiation and convection: Δ

$$T_N^{i+1} = T_N^i + \frac{2 \cdot \Delta t}{(\rho c)_N^i \cdot \Delta x} \cdot \left[\left(\frac{\lambda_{N-1}^i + \lambda_N^i}{2} \right) \cdot \left(\frac{T_{N-1}^i - T_N^i}{\Delta x} \right) - \varepsilon \sigma \left({T_N^i}^4 - T_\infty^4 \right) - h_c^i \left(T_N^i - T_\infty \right) \right] \qquad (5)$$

where T_N^{i+1} is the temperature of concrete at the node of the unexposed surface in the subsequent timestep, *K;*

T_N^i is the temperature of concrete at the node of the unexposed surface in the present timestep, *K*;

$\lambda_{N-1,N}^i$ is the thermal conductivity of concrete at nodes *N-1* and *N* at present temperature, *W/m K;*

h^i is the convective heat transfer coefficient;

T_∞ is the ambient temperature, *K.*

The convective heat transfer coefficient at the exposed and unexposed faces of a specimen for a standard furnace test which are used in previous equations can be calculated as (Bergman, et al., 2016):

$$h_c^i = \frac{\overline{Nu}_L \cdot k_{air}}{L} \tag{6}$$

For the case of an upper surface of a horizontal hot plate recommended correlations for the average Nusselt number are:

$$\overline{Nu}_L = \begin{cases} 0.54 \cdot Ra_L^{1/4}, & 10^4 \leq Ra_L \leq 10^7 \\ 0.15 \cdot Ra_L^{1/3}, & 10^7 < Ra_L \leq 10^{11} \end{cases} \tag{7}$$

For the case of a lower surface of a horizontal hot plate recommended correlations for the average Nusselt number are:

$$\overline{Nu}_L = 0.52 \cdot Ra_L^{1/5}, \ 10^4 \leq Ra_L \leq 10^9 \tag{8}$$

$$Ra_L = \frac{g \cdot \beta_{air} \cdot (T_N^i - T_{amb}) \cdot L^3}{v_{air} \cdot \alpha_{air}} \tag{9}$$

where T_N^i is the temperature of concrete at the node of the unexposed surface in the timestep *i*, *K*;

g is the acceleration of gravity, *9.81 m/s²;*

L is the length of the unexposed face of a specimen, *m*.

The volumetric thermal expansion coefficient of air which shows the variations in density of air as a reaction to temperature changes is expressed as:

$$\beta_{air} = \frac{1}{T_f} \tag{10}$$

The temperature of the boundary layer (film temperature) is found as:

$$T_f = \frac{(T_N^i + T_{amb})}{2} \tag{11}$$

The temperature-dependant terms of thermal conductivity (k_{air}), kinematic viscosity (v_{air}), and thermal diffusivity (α_{air}) are adopted from the Lagrangian polynomial approximations derived by Maluk (Maluk, 2014) and verified with the tabulated data in (Bergman, et al., 2016):

$$k_{air}(T_f) = -2.471 \times 10^{-20} \cdot T_f^6 + 1.277 \times 10^{-16} \cdot T_f^5 - 2.326 \times 10^{-13} \cdot T_f^4 + 2.1121 \times 10^{-10} \cdot T_f^3 - 1.363 \times 10^{-7} \cdot T_f^2 + 1.240 \times 10^{-4} \cdot T_f - 2.733 \times 10^{-3} \tag{12}$$

$$v_{air}(T_f) = -1.236 \times 10^{-22} \cdot T_f^6 + 6.636 \times 10^{-19} \cdot T_f^5 - 1.366 \times 10^{-15} \cdot T_f^4 + 1.359 \times 10^{-12} \cdot T_f^3 - 6.066 \times 10^{-10} \cdot T_f^2 + 2.172 \times 10^{-7} \cdot T_f - 2.164 \times 10^{-5} \tag{13}$$

$$\alpha_{air}(T_f) = -1.497 \times 10^{-22} \cdot T_f^6 + 7.581 \times 10^{-19} \cdot T_f^5 - 1.373 \times 10^{-15} \cdot T_f^4 + 1.111 \times 10^{-12} \cdot T_f^3 - 3.187 \times 10^{-10} \cdot T_f^2 + 1.556 \times 10^{-7} \cdot T_f - 1.601 \times 10^{-5} \tag{14}$$

The described finite difference heat transfer model can be used to model the process of heat transfer inside a thermally thick body and to study the temperature gradients at any timestamp of the heating process.

2.4.2 Incident heat flux

As the array of radiant panels of H-TRIS is aligned centre-to-centre both vertically and horizontally with a concrete specimen, the problem of heat transfer through the concrete body is simplified to one-dimensional along the centreline of a specimen. The energy balance, in this case, will include the incident heat flux which goes into the absorbed (or net) heat flux and convective and radiative losses (Fig. 12).

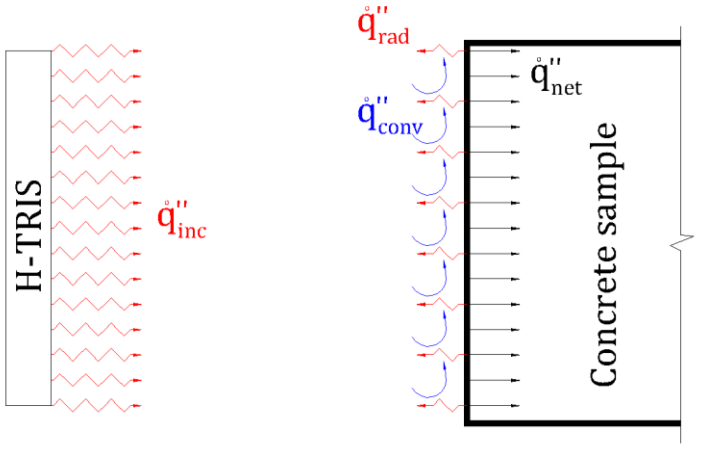

Figure 12. Energy balance of a test sample

The mathematical representation of the energy balance in this case can be viewed as:

$$\varepsilon \dot{q}''^{\,i}_{inc} = \dot{q}''^{\,i}_{net} + \dot{q}''^{\,i}_{rad} + \dot{q}''^{\,i}_{conv} \tag{15}$$

where ε is the emissivity of the specimen's surface;

$\dot{q}''^{\,i}_{inc}$ is the incident heat flux, radiated by H-TRIS apparatus, W/m^2;

$\dot{q}''_{net}$ is the net heat flux to the concrete specimen, W/m^2;

$\dot{q}''^{\,i}_{rad}$ is the radiative losses from the exposed surface of concrete specimen, W/m^2;

$\dot{q}''^{\,i}_{conv}$ is the convective losses from the exposed surface of concrete specimen, W/m^2.

Radiative losses from the vertical surface of a test specimen can be found as:

$$\dot{q}''^{\,i}_{rad} = \varepsilon\sigma\left(T_1^{i\,4} - T_{amb}^{i\,4}\right) \tag{16}$$

where ε is the emissivity of the specimen's surface;

σ is the Stefan–Boltzmann constant, 5.67×10^{-8} W/m^2K^4;

T_1^i is the temperature of the exposed surface, K;

T_{amb}^i is the ambient temperature, K.

Convective losses from the vertical surface of a test specimen can be found as:

$$\dot{q}''^{\,i}_{conv} = h_c^i \cdot \left(T_1^i - T_{amb}\right) \tag{17}$$

where h_c^i is the convective heat transfer coefficient, W/m^2K.

T_1^i is the temperature of the exposed surface, K;

T_{amb}^i is the ambient temperature, K.

The convective heat transfer coefficient can be calculated as for a vertical hot surface in accordance with (Bergman, et al., 2016):

$$h_c^i = \frac{\overline{Nu}_L \cdot k_{air}}{L} \tag{18}$$

Correlations for the average Nusselt number are taken for the case of convection near a vertical plate in a laminar or combined laminar and turbulent flow depending on the Rayleigh number (Bergman, et al., 2016):

$$\overline{Nu}_L = \begin{cases} 0.68 + \frac{0.670 \cdot Ra_L^{1/4}}{\left[1+(0.492/Pr)^{9/16}\right]^{4/9}}, & Ra_L \leq 10^9 \\ \left[0.825 + \frac{0.387 \cdot Ra_L^{1/6}}{\left[1+(0.492/Pr)^{9/16}\right]^{8/27}}\right]^2, & Ra_L > 10^9 \end{cases} \tag{19}$$

The Rayleigh number itself is calculated as:

$$Ra_L = \frac{g \cdot \beta_{air} \cdot (T_1^i - T_{amb}) \cdot L^3}{v_{air} \cdot \alpha_{air}} \tag{20}$$

And Prandtl number is found as a function of film temperature:

$$Pr(T_f) = \frac{v_{air}(T_f)}{\alpha_{air}(T_f)} \tag{21}$$

Where T_f is the arithmetic mean temperature between the exposed surface and the ambient air:

$$T_f = \frac{(T_1^i + T_{amb})}{2} \tag{22}$$

Using the procedure described above the time history of incident heat flux can be calculated and later be used to program the H-TRIS apparatus to follow the defined temperature-time curve replicating the conditions inside a standard furnace.

2.4.3 Temperatur-dependent properties of concrete

As concrete is a composite material its properties change with temperature (Ma, et al., 2015). Upon heating concrete experiences changes starting from moisture evaporation and ending at the decomposition of its components. Thus, changes in specific heat, density and thermal conductivity are tied with those processes. A study by Zhang et al. (Zhang, et al., 2014) generalized the change of properties of concrete such as compressive and tensile uniaxial strength, elastic modulus, Biot's number with temperature. The work shows that the dehydration and decrease of the tensile strength of concrete start at ~105°C. The compressive strength starts to decrease after heating to 200°C.

In the abovementioned calculations of the finite difference heat transfer model, the temperature-dependent properties of concrete were taken from the Eurocode (BS EN 1992-1-2:2004,). Specific heat was calculated as:

$$c_p(\theta) = \begin{cases} c_p(\theta) = 900, \ 20℃ \leq \theta \leq 100℃ \\ c_p(\theta) = 2020, \ 100℃ < \theta \leq 115℃ \\ c_p(\theta) = (2020 - (\theta - 115) \cdot 12), \ 115℃ < \theta \leq 200℃ \\ c_p(\theta) = 1000, \ 200℃ < \theta \leq 1200℃ \end{cases} \tag{23}$$

where $c_p(\theta)$ is the specific heat of concrete, *J/kg K*;

θ is temperature of concrete, ℃.

The variation of density of concrete is defined by the loss of moisture during the exposure to heat and was calculated as:

$$\rho(\theta) = \begin{cases} \rho(\theta) = \rho(20℃), \ 20℃ \leq \theta \leq 115℃ \\ \rho(\theta) = \rho(20℃) \cdot (1 - 0.02(\theta - 115)/85), \ 115℃ < \theta \leq 200℃ \\ \rho(\theta) = \rho(20℃) \cdot (0.98 - 0.03(\theta - 200)/200), \ 200℃ < \theta \leq 400℃ \\ \rho(\theta) = \rho(20℃) \cdot (1 - 0.07(\theta - 400)/800), \ 400℃ < \theta \leq 1200℃ \end{cases} \quad (24)$$

where $\rho(\theta)$ is the density of concrete, kg/m^3.

Thermal conductivity was calculated as an average between the lower and the upper limits. The upper limit was calculated as:

$$\lambda_c(\theta) = 2 - 0.2451(\theta/100) + 0.107(\theta/100)^2 , \ 20℃ < \theta \leq 1200℃ \quad (25)$$

where $\lambda_c(\theta)$ is the thermal conductivity of concrete, $W/m\ K$.

The lower limit of thermal conductivity of concrete was calculated as:

$$\lambda_c(\theta) = 1.36 - 0.136(\theta/100) + 0.0057(\theta/100)^2 , \ 20℃ < \theta \leq 1200℃ \quad (26)$$

The developed heat transfer finite difference model was later checked by providing the ISO 834 fire curve as the input parameter. The received temperature gradients at different depths of the body were compared with isotherms for concrete slabs provided in Eurocode (BS EN 1992-1-2:2004,). The comparison showed very good convergence.

This page is intentionally left blank

CHAPTER 3. RESULTS OF EXPERIMENTAL TESTING

3.1 Calibration of the H-TRIS apparatus

Prior to the experimental testing, the H-TRIS apparatus was calibrated with the help of a heat flux gauge. The calibration process involved the building of the dependence of the incident heat flux from the distance between the array of H-TRIS radiant panels and the tip of the heat flux gauge. The gauge was placed in such location of the set-up that the distance from its tip to the radiant panels was equal to the distance from the exposed surface of a concrete sample to the radiant panels of H-TRIS. Also, the tip of the gauge was located placed in such way that the convective and conductive heating mechanisms were eliminated. The calibration curve is presented in Fig. 13.

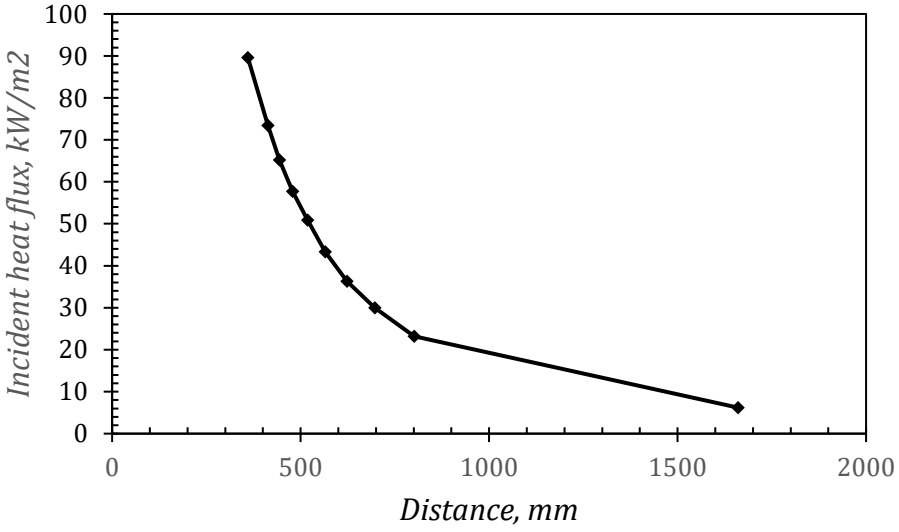

Figure 13. Calibration curve of H-TRIS apparatus

As it can be seen from the plot, the calibration curve has an asymptotic shape and has a significant increase in the incident heat flux, once it gets closer to the exposed surface. Such behaviour of the dependence can be explained by the equation of radiative heat transfer, where the heat flux depends from the squared value of distance. Also, for that reason the H-TRIS apparatus is programmed in such way that it takes more data point when it gets closer to the exposed surface, approximating the dependence into a linear function between the 1st and the 2nd points.

3.2 Strains on the exposed surface

The analysis of the data from the measurement of vertical strains on exposed surfaces of concrete samples showed that the maximum strains were measured by the strain gauges in the centres of samples. Hence, those measurements were taken for further analysis and are presented in Fig 14. It should be noted, that some of the strain gauges were excluded from the analysis due to abnormal readings. This could happen due to bad glueing, soldering or concrete surface unevenness.

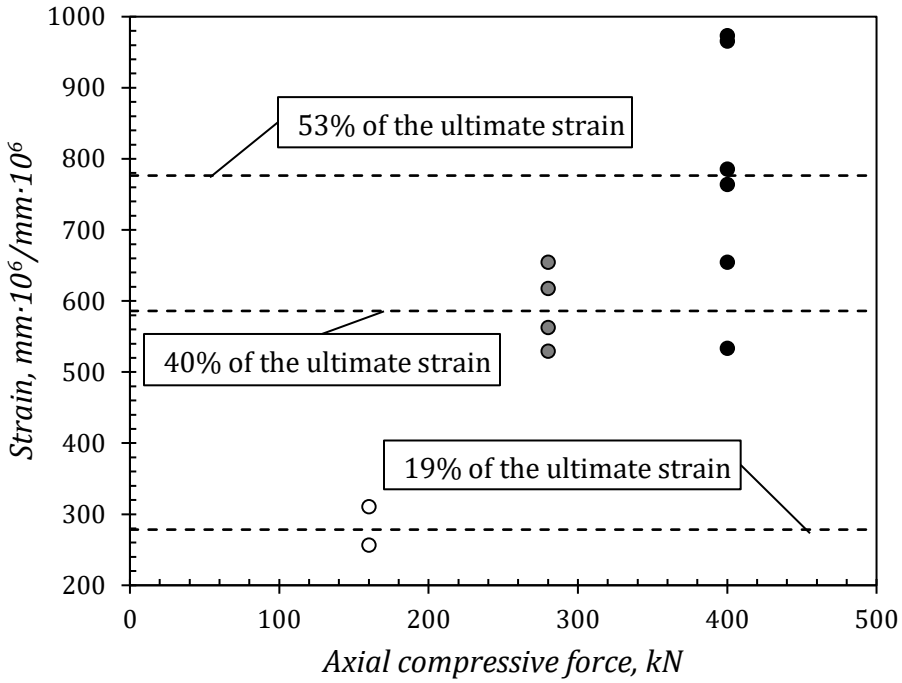

Figure 14. Strains in the centres of exposed faces of concrete samples

The dashed lines in the figure above represent the average values of vertical strains measured in centres of the concrete specimens with strain gauges under defined compressive forces. These values are presented as a proportion of the ultimate strain which corresponds to the compressive cylindrical strength of the concrete mix. Also, these calculated averages of vertical strains were used in labelling of samples. The correspondence of the measured strains to stresses and proportions of the ultimate strain is presented in Table 8.

Table 8. Average mechanical parameters in the centres of the exposed face of samples

Compressive force, kN	**Average stress, MPa**	**Average strain, mm·10⁶/mm·10⁶**	**% of concrete ultimate strain**
160	10.8	284	19
280	22.5	591	40
400	29.6	780	53

A total of 18 samples were tested during experimental research. Only 6 of them experienced spalling. The summary of all tested samples made of plain concrete is presented in Table 9.

Table 9. Summary of test data of plain concrete samples

Compressive force	**O = 0.0415 m$^{1/2}$**	**O = 0.0515 m$^{1/2}$**	**O = 0.1 m$^{1/2}$**
No load	HC0.415_L0%_PP0.0_1 *No spalling* (26.5 min) HC0.415_L0%_PP0.0 *No spalling* (60 min)	HC0.0515_L0%_PP0.0 *No spalling* (40 min)	—
160 kN	HC0.0415_L19%_PP0.0 *No spalling* (40 min)	—	HC0.1_L19%_PP0.0 *Spalling* (11 min)
280 kN	HC0.0415_L40%_PP0.0 *No spalling* (40 min)	HC0.0515_L40%_PP0.0 *No spalling* (40 min)	HC0.1_L40%_PP0.0 *Spalling* (6 min) HC0.1_L40%_PP0.0_1 *Spalling* (7 min)
400 kN	HC0.0415_L53%_PP0.0 *Spalling* (21.5min) HC0.0415_L53%_PP0.0_1 *Spalling* (18 min) HC0.0415_L53%_PP0.0_2 *Spalling* (22 min)	—	—

As it can be seen from the table above, spalling occurred only in samples exposed to the heating conditions which correspond the opening factors *O = 0.0415 m$^{1/2}$* and *O = 0.1 m$^{1/2}$*. However, samples were not exposed to some of the combinations of compressive loading – heating conditions, thus making the occurrence of spalling in such conditions undefined.

The results of the occurrence spalling in samples with the inclusion of 1.6 kg/m^3 PP fibres in the mix are presented in Table 10.

Table 10. Summary of test data of concrete samples with 1.6 kg/m^3 of PP fibres

Compressive force	**O = 0.1 m$^{1/2}$**	**O = 0.2 m$^{1/2}$**
280 kN	HC0.1_L40%_PP1.6 *No spalling* (30 min) HC0.1_L40%_PP1.6_1 *No spalling* (30 min)	—
400 kN	HC0.1_L53%_PP1.6 *No spalling* (30 min) HC0.1_L53%_PP1.6_1 *No spalling* (30 min)	HC0.2_L53%_PP1.6 *No spalling* (30 min) HC0.2_L53%_PP1.6_1 *No spalling* (30 min)

The data presented in the tables above shows that no spalling occurred at concrete samples with the inclusion of PP fibres in the mix.

3.3 Vertical cracks

As it was mentioned before, the tests of concrete samples began with the application of compressive load. No visible reactions to the loading such as cracks or flaking were noticed on any samples at any levels of loading. At load levels which corresponded to 40% and 53% of the ultimate strain of concrete at all heating conditions, vertical cracks appeared on both side faces of concrete samples (Fig. 15).

Such behaviour can be tied with the increase of stress gradient between the compressed and not compressed parts of a concrete sample due to eccentrically applied load and self-restraint of a sample. Hence, the increase is due to the heating of the compressed part and thus increase of compressive stresses in that part due to the thermal expansion.

Such cracks appeared at initial stages of heating at about 5-7 minutes of the slowest heating (*O = 0.0415 m$^{1/2}$*) and at about 3-4 minutes of the fastest heating (*O = 0.2 m$^{1/2}$*) before the spalling or the start of moisture escape. The cracks could be prevented if the reinforcement was introduced in the concrete cross-section which could take the tensile stresses. Also non-eccentrical uniform compressive loading would be beneficial in preventing the cracking. However, an actuator of higher capacity will be needed.

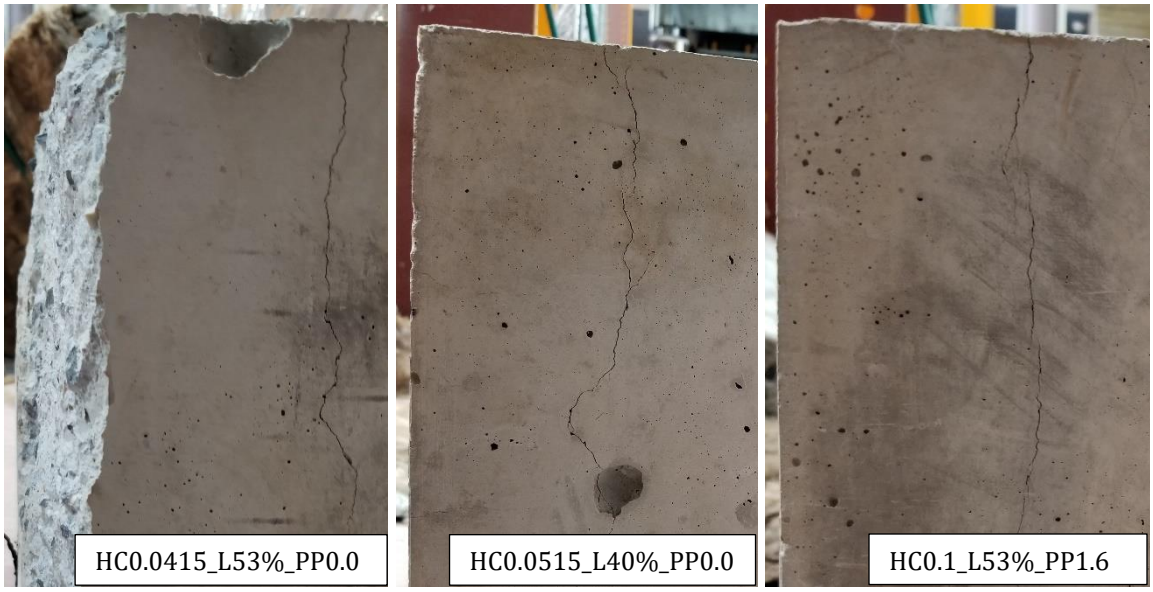

Figure 15. Vertical cracks on side faces of concrete samples

As it can be seen from the picture above, vertical cracks had similar pattern and location across all the samples. This shows that the point of the application of the compressive force defined the location of the sharp stress gradient which resulted in the formation of the cracks.

3.4 Escape of moisture

The average moisture content of the tested samples constituted 3.7%. Upon heating, the moisture tends to migrate deeper into the concrete body to the lower temperature. However, this process is 3-dimensional and the moisture spreads not only in the direction from the exposed face to the back face but also to the side, bottom and upper faces due to increased pore pressure in the central part and the formation of a "moisture clog".

At the slowest heating conditions ($O = 0.0415\ m^{1/2}$) the moisture appeared in liquid form on the side faces at ~19 minutes of heating (Fig. 16). With the increase in the rate of heating, the time of moisture appearance decreased. So, at $O = 0.0515\ m^{1/2}$ the moisture appeared at ~17 minutes and at $O = 0.1\ m^{1/2}$ – close to the spalling time which is 7-11 minutes. However, the spalling of the sample HC0.1_L40%_PP0.0 occurred before any moisture was noticed at side faces.

It should be noted, that the behaviour of moisture in the samples with 1.6 kg/m^3 PP fibres in the mix was different. At the same heating and loading conditions ($O = 0.1\ m^{1/2}$, *40% of the concrete ultimate strain)* no moisture was noticed on any face of concrete samples other than

the back face (Fig. 16). This indirectly shows higher permeability of such concrete which worsens the conditions for the formation of a "moisture clog". Also, under the heaviest loading conditions (*53% of the ultimate concrete strain*) the moisture appeared on all faces of specimens except the exposed face. This shows the negative influence of compressive loading on the distribution of free water towards the back face.

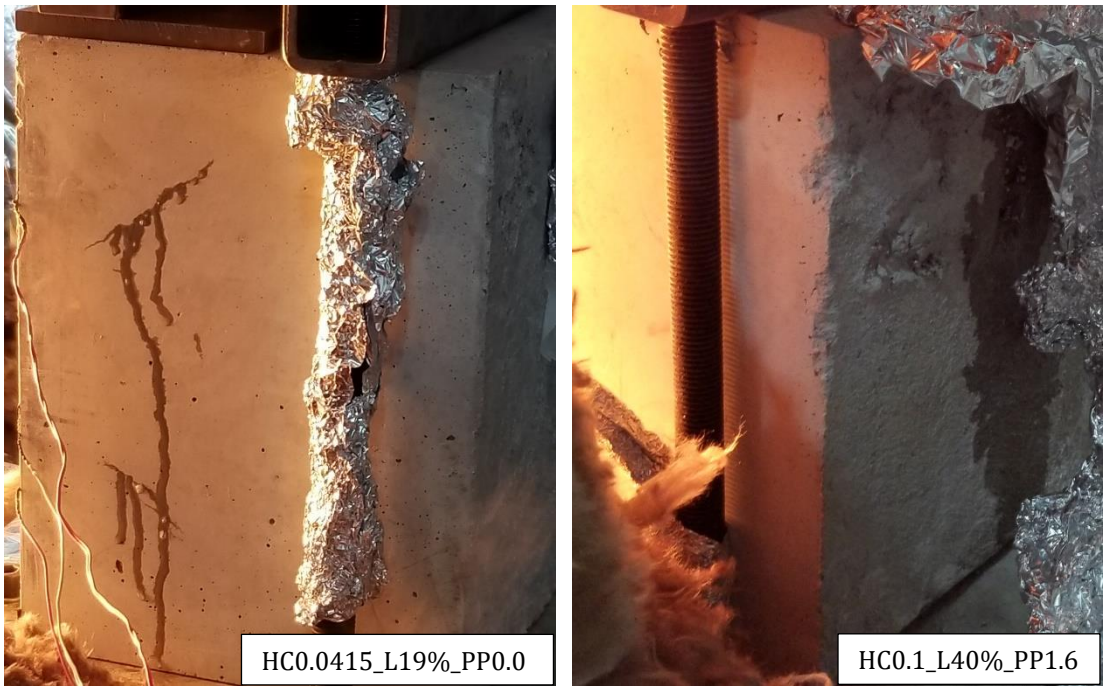

Figure 16. Escape of moisture from concrete samples during testing from a side face (HC0.0415_L19%_PP0.0) and from a back face (HC0.1_L40%_PP1.6)

3.5 Occurrence of spalling

As it was mentioned before, spalling occurred only at 6 samples out of total 18 under 3 different conditions of heating and compressive loading. However, the pattern and the severity of spalling was not the same across the samples. At the slowest heating conditions and highest loading conditions (*O = 0.0415 $m^{1/2}$, 53% of the concrete ultimate strain*) the spalling was one-time and accompanied by a loud bang sound. The depth of spalling varied between 9 mm and 21 mm with an average value of 15 mm. Also, it should be noted, that the sample HC0.0415_L53%_PP0.0_1 experienced deeper spalling than the other two spalled samples with an average depth of 20mm. The views of the front faces of spalled concrete samples are presented in Fig. 17.

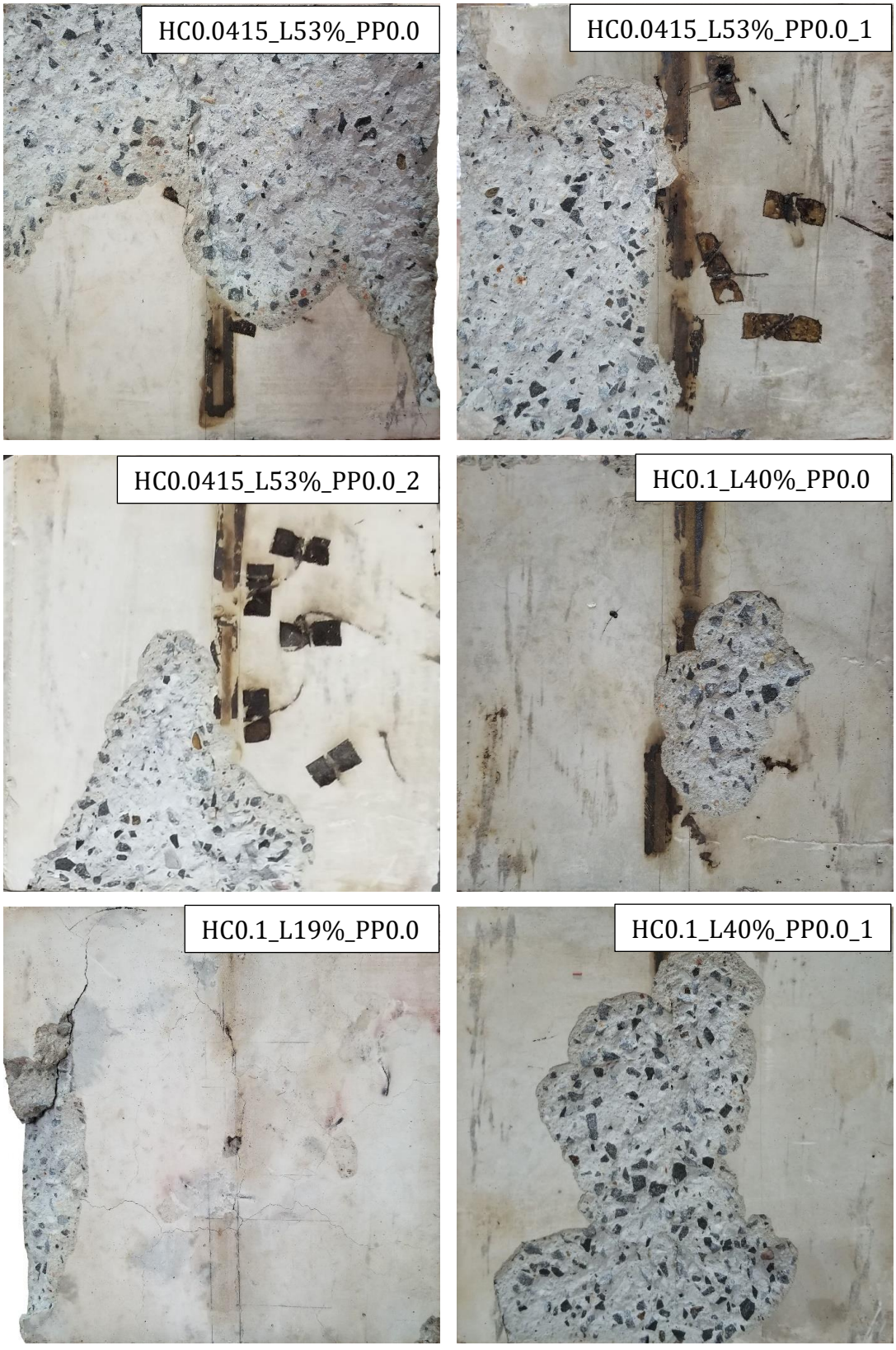

Figure 17. View of the front faces of spalled concrete samples after testing

On the other side, more severe heating conditions and lower loading led to less severe spalling. This means that the bang sounds were a lot quieter and the spalling depth was less. Apart from that, the spalling effect was progressive: after the first occurrence, the next one occurred after ~5 seconds before the heaters were turned off. The spalling depth varied between 5 mm and 8 mm with an average value of 6.5 mm. It should be noted that the sample HC0.1_L19%_PP0.0 spalled at the side edge and was excluded from those measurements.

As it can be seen from the pictures above, spalling had random pattern and shifted the focus in all directions. Apart from that, the amount of spalled concrete and the affected depth were different too.

3.6 Temperature measurements

All the concrete samples were equipped with thermocouples located at a range of distances from the exposed surface. The full description of each sample can be found in Appendix A. The readings from thermocouples allowed to record temperature-time histories at those distances and to build the temperature gradients at any timestamp of a test. However, not all thermocouples showed adequate temperature readings due to shifting in the time of casting. Apart from that, many of them were damaged and didn't show any readings. Thus, further analysis is based on the data available and is structured in accordance with heating conditions.

3.6.1 "Slow" heating conditions

The experimental temperature-time curves in a range of distances from the exposed surfaces with superimposed theoretical curves which were calculated with the help of finite difference heat transfer model are presented in Fig. 18.

In the slowest heating conditions with the opening factor $O = 0.0415\ m^{1/2}$, the development of temperature in the concrete body was analysed. All of the samples showed very close to theoretical results at the distances of 10 mm, 30 mm and 50 mm from the exposed surface. Apart from that, the convergence with the theoretical curves, calculated using the finite difference method, is also good at the first ~15 minutes of heating.

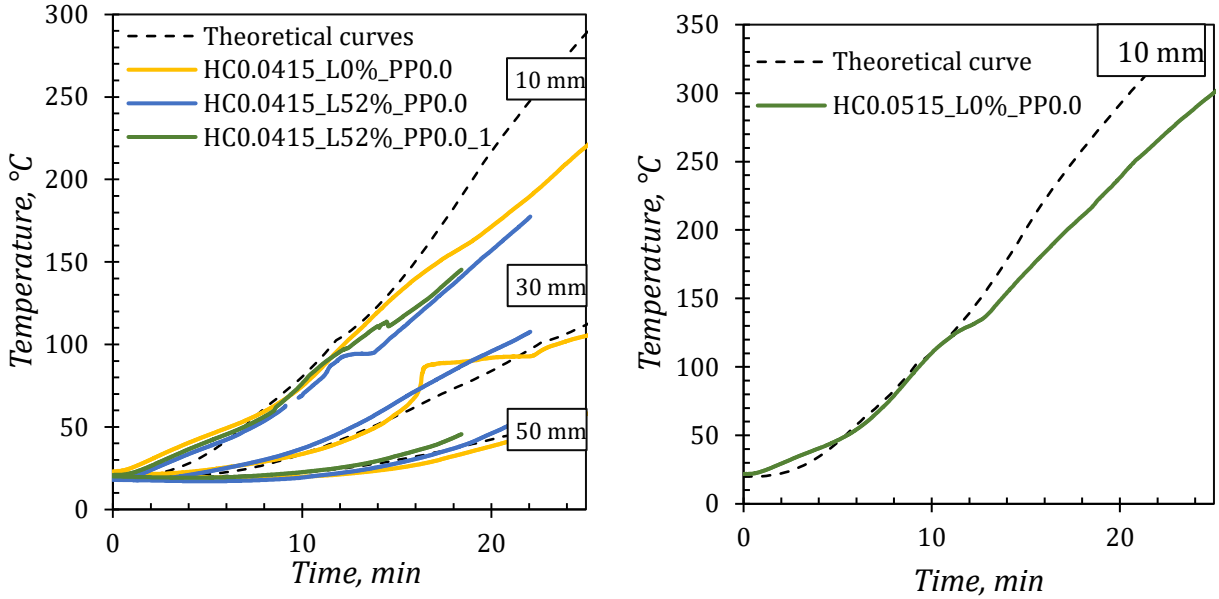

Figure 18. Experimental temperature-time history curves in comparison with theoretical curves with $O = 0.0415\ m^{1/2}$ and $O = 0.0515\ m^{1/2}$

However, after the 15-minute timestamp, the measured values at 10 mm tend to go lower than the theoretical ones. Such behaviour can be explained by the beginning of moisture migration deeper into the body of concrete at that period of the test. It is known that the appearance of liquid moisture on the sides of samples occurred soon after that, namely at ~19 minutes. So, the hot migrating moisture transferred energy from the exposed surface towards the back face and to the sides. Apart from that, the water from the sides evaporated quickly after the appearance, taking the energy from the heated sample.

Another possible reason for such mismatch of the theoretical and experimental curves at 10 mm distance is that the heat transfer model accounts for concrete thermal properties with constant moisture content and doesn't account for the moisture migration and further evaporation from sample's faces. Also, the exact locations of thermocouples were uncertain due to their possible shifting during casting.

For the heating conditions with the opening factor $O = 0.0515\ m^{1/2}$ the data from only one thermocouple out of 2 samples were available for analysis. As it can be seen from Fig. 18 the same mismatch as in previous heating conditions between the experimental and the theoretical curves is observed at ~12 minutes.

Using the finite difference heat transfer model the theoretical temperature gradients at different timestamps were plotted with superimposed experimental data points and are presented in Fig. 19.

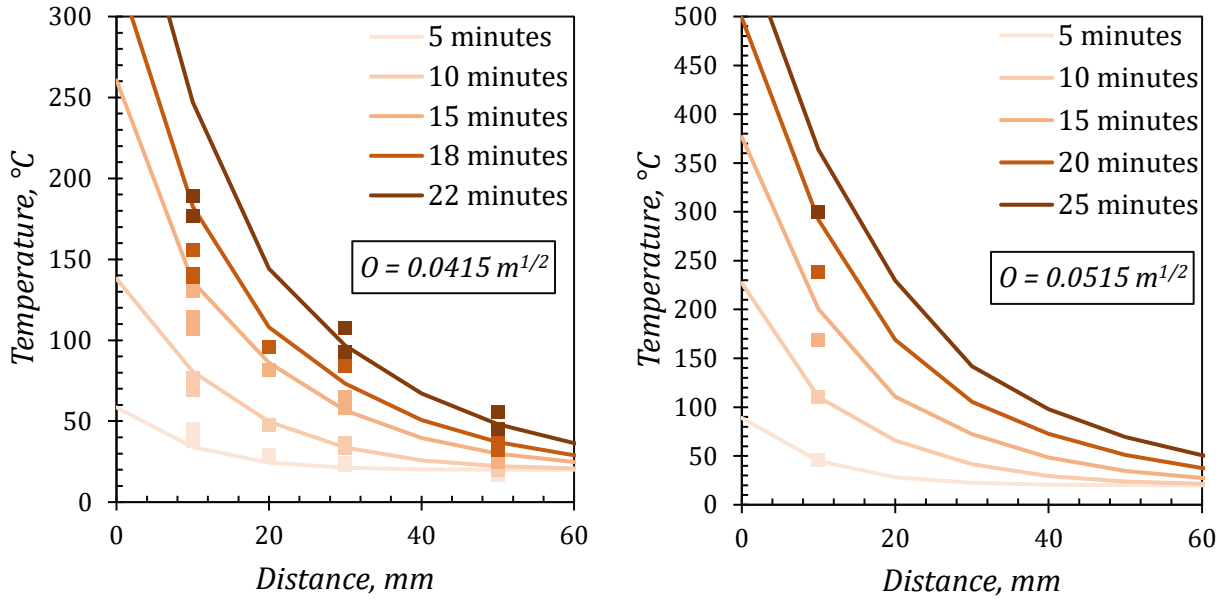

Figure 19. Theoretical temperature gradients with superimposed experimental data points

Experimental data points deviate from theoretical temperature gradients and the deviations increase with time and decrease with distance. The decrease of temperature deviations with distance can be explained in such way that the sensitivity of temperature change with the increment in distance is smaller and the shifting of thermocouples does not play such important role deeper in concrete than near the exposed surface

3.6.2 "Fast" heating conditions

For the faster heating conditions with the opening factor $O = 0.1\ m^{1/2}$, the proposed theoretical model showed good convergence with the experimental data. In the tests with such heating conditions, two samples experienced spalling at 6 and 7 minutes of testing. For this reason, the temperature-time history graphs are presented in two versions: for the first 8 minutes of testing prior to the spalling of samples without PP fibres in the mix, and full 30-minute curves of not spalled samples with 1.6 kg/m^3 PP fibres (Fig. 20).

The development of temperature gradients prior to the occurrence of spalling is presented in Fig. 21.

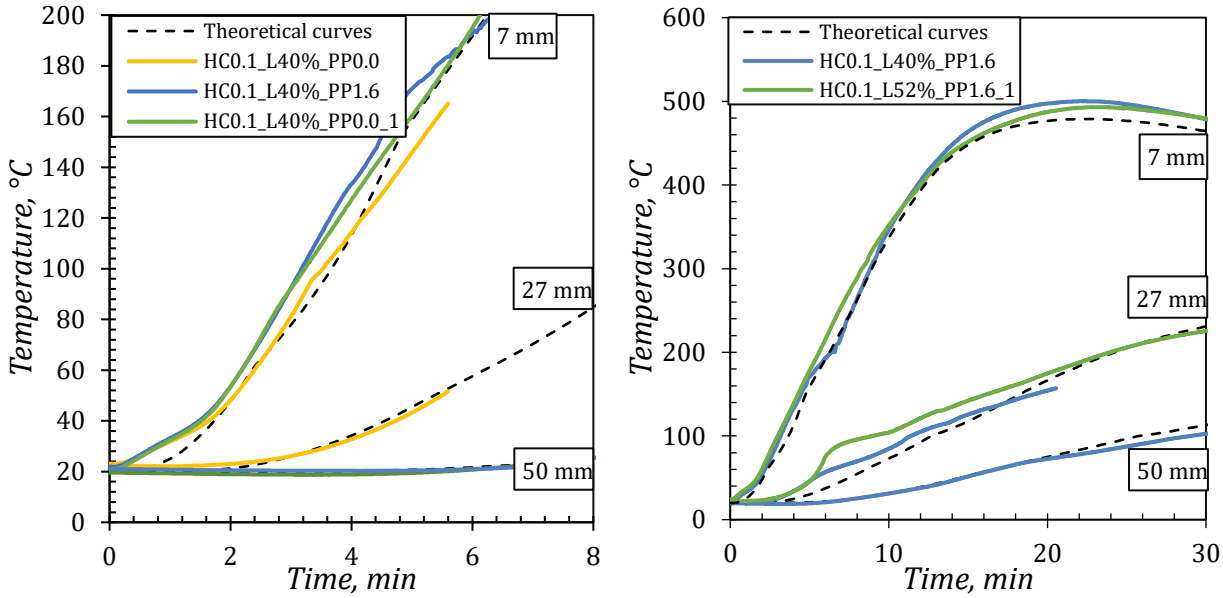

Figure 20. Experimental temperature-time history curves in comparison with theoretical curves with $O = 0.0515\ m^{1/2}$

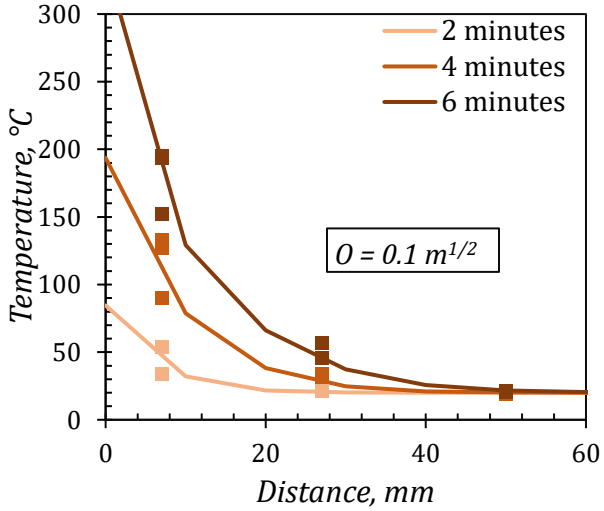

Figure 21. Temperature gradients at different timestamps of test

As it can be seen from the temperature gradients above, the prediction of the theoretical model worked better for faster heating conditions. However, in comparison with "slow" heating conditions, only the first 6 minutes of heating exposure were compared. It means that the moisture migration process was just beginning and hasn't undergone full development thus not influencing the heat transfer processes in the concrete body.

Unfortunately, no correct readings were received for any samples exposed to the fast heating conditions with the opening factor $O = 0.2\ m^{1/2}$.

This page is intentionally left blank

CHAPTER 4. DISCUSSION

The analysis of the experimental data allowed to receive the dependence of heating conditions dictated by the opening factor of a parametric fire together with sustained loading conditions on the occurrence of concrete spalling. The proposed diagram is presented in Fig. 22.

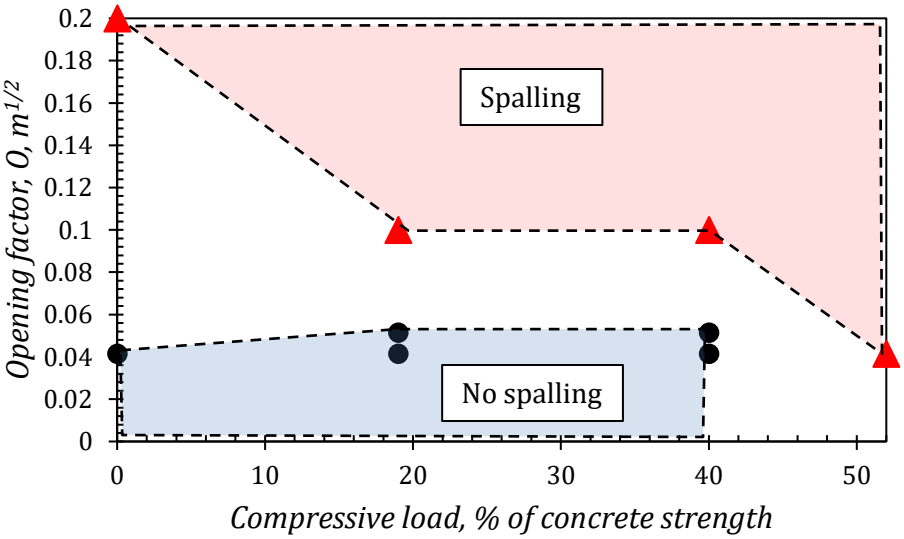

Figure 22. Influence of the opening factor and sustained compressive load on the occurrence of spalling

The red region on the diagram shows the region which denotes the conditions under which concrete spalling is likely to occur. On the other side, the blue region defines the conditions when the occurrence of spalling will not be expected. The white region between those mentioned two covers the boundary area where any of the conditions may occur and where additional data points are required.

The diagram shows that the propensity of concrete to spalling increases with the increase of compressive loading and of the severity of fire conditions, which are expressed as the opening factor value.

It should be noted, that the abovementioned diagram is based solely on the research of the particular concrete mix, after long ageing time (309 days). The described dependence from the conditions can be inapplicable for other types of concrete samples. However, a certain trend can be noticed from the diagram: the increase in sustained compressive loading

leads to decreased opening factor needed for spalling to occur. This means that less severe fire can lead to the occurrence of spalling if a structure is more heavily loaded.

Other than external actions, the internal reactions of concrete caused by those actions can help to understand the internal conditions which correspond to spalling. Such conditions can be certain thermal gradients that are developed at the time of spalling in the concrete body. To study this possible dependence, temperature gradients in the timestamp of spalling were plotted on one graph shown in Fig. 23. These gradients are developed using the finite difference heat transfer model.

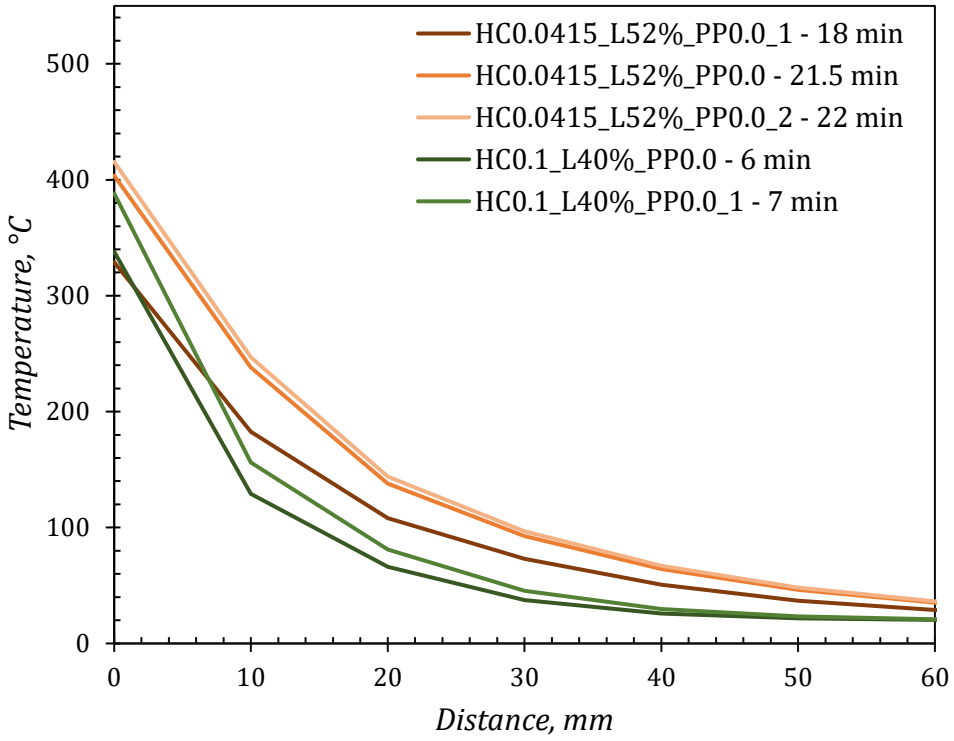

Figure 23. Temperature gradients which were theoretically developed in concrete samples in the timestamp of spalling

As it can be seen from the graph above, temperature gradients in different spalled concrete samples appear to have similar surface temperatures from 320℃ to 419℃. However, the temperature gradient of the sample HC0.1_L19%PP0.0 was eliminated from the analysis because of the abnormal pattern of spalling – a spalled edge.

Taking into account the variability of properties of concrete samples, surface temperatures and temperature gradients appear to have very close values. An interesting

fact is that spalled samples subjected to very different fire exposures (fast and slow) showed very similar temperature gradients in the time of spalling. It means that such conditions should be avoided in the type of concrete samples studied in order to prevent the occurrence of spalling.

Apart from temperature gradients, another parameter that can potentially characterize the propensity to spalling of a concrete sample is the amount of radiant energy that was absorbed through the exposed surface. These values were calculated as the areas under the graphs of the net heat flux presented in Fig. 10 limited by the timestamps when spalling events occurred.

Also, temperature differences at the average spalled depths were analysed and are presented in Table 11. These differences were calculated between the exposed surfaces and the corresponding spalled depths at timestamps of observed spalling events.

Table 11. Thermal properties of spalled samples

Sample label	Average spalling depth, mm	Time to spalling, min	Energy absorbed, MJ	Temperature difference at spalling depth, *°C*	Temperature at spalling depth, *°C*
HC0.0415_L53%PP0.0	15	21.5	18,2	216	188
HC0.0415_L53%PP0.0_1	20	18	13,6	221	108
HC0.0415_L53%PP0.0_2	15	22	19,4	221	198
HC0.1_L40%PP0.0	6.5	6	8,7	136	202
HC0.1_L40%PP0.0_1	6.5	7	11	151	237

It can be seen from the table above that for two different heating regimes ($O = 0.0415\ m^{1/2}$ and $O = 0.1\ m^{1/2}$) there are distinguishable differences between the amounts of energy absorbed and temperature differences at spalling depths. These differences were also physically observed during the tests. Spalling of samples with the opening factor $O = 0.0415\ m^{1/2}$ was one-time, explosive and deep, whereas the other group showed progressive spalling with a lot less loud bang sounds and smaller spalling depths. These circumstances show that the heating rate of fire plays an important role in the occurrence of spalling, its depth and type. The bigger the heating rate the more probability of progressive spalling with

less time to spalling, smaller spalling depths and less energy absorbed. On the other hand, fires with slower heating rates induce higher temperature differences at the spalling depths.

The analysis of temperatures at the depth of spalling showed the range from 188°*C* to 237°*C*. According to (Liu, et al., 2018) such temperatures correspond to thermo-hygral spalling type. However, the only particular spalling mechanism can never clearly occur without the influence of other mechanisms. In present research the thermo-mechanical mechanism had a clear influence due to the applied mechanical loading. However, the thermal expansion of concrete did not contribute to the development of stresses in vertical direction near the exposed faces of the samples because the loading was applied by means of the hydraulic actuator which was force-controlled. It means that it allowed the sample to expand without the increase in compressive stress. Thus, it can not be considered as a restrained structure.

Regardless the unrealistic mechanical boundary conditions the test allowed to study the occurrence of spalling under sustained loading and constant compressive stress. This data will be useful for structural fire safety engineers in the process of the analysis of a structure when the compressive stresses due to thermal expansion are known and temperature gradients can also be calculated using the finite difference heat transfer model.

4.1 Comparison of the results with other researchers

As it was mentioned before, exactly the same concrete samples were tested in the research performed by Thorne (Thorne, 2018). In that research, the heating curve called "long-cold" is equal to the heating curve with the opening factor $O = 0.0415\ m^{1/2}$ in the present research. However, there are substantial differences in the experimental results. Thus, the unloaded samples and samples subjected to the loading levels of up to 40% of concrete ultimate strain did not spall while those tested by Thorne spalled.

Such different behaviour of concrete samples may be explained by the different age of concrete. Thorne's samples were dried for 146 days until testing while the samples in the present research were dried for 309 days. It is known that the degree of pore saturation (DPS) decreases with concrete ageing thus decreasing the risk of thermo-hygral spalling (Liu, et al., 2018).

On one hand, the processes of hydration and carbonation, which take place in concrete for a long period of time, close and narrow the pores and interconnections between them with the carbonation and hydration products which leads to the decrease of permeability. On the other hand, the processes of drying and shrinking induce microcracks and leave empty channels upon the escape of water vapour. Such processes clearly increase the permeability (Sanjuán & Muñoz-Martialay, 1995). The domination of any of these processes depends on the curing conditions and concrete mix design. The present research implicitly showed that the permeability most likely increased with age because the concrete became less prone to spalling.

There is still no agreement among researchers considering the influence of ageing of concrete on its propensity to spalling. In the research by Jansson and Boström (Jansson & Boström, 2013) 3 concrete mixes out of 4 showed higher propensity to spalling with ageing while the 4th one showed the opposite result. This brings the idea that the ageing of concrete can't be viewed solely as the factor of influence but it should be considered together with other factors such as concrete mix design, conditions of drying or shape of a sample. If under the term "ageing" stands the process of continuous hydration of cement inside the concrete body together with its shrinkage and escape of moisture, then the best characteristic for the description of the moisture inside the concrete body and its distribution along the network of microchannels and pores will be the degree of pore saturation (DPS).

Regardless of the difference in the age of concrete samples, the types of concrete spalling remained the same for both pieces of research: faster heating rates resulted in progressive spalling with lower depths while slower heating led to one-time more severe spalling.

Sustained compressive stresses which influence the occurrence of spalling were compared with those discussed in the research by Rickard et. al. (Rickard, et al., 2017). In the discussed research the sustained compressive stress over 10 MPa facilitated the occurrence of spalling while in present research only stresses over 29.6 MPa influenced the effect. However, such comparison is not fully correct due to different concrete used and heating curves applied. Also, in present research, there was a gradient of compressive stress throughout the depth of the sample due to the eccentrically applied load.

Results, similar to ones in present research were received by Carré et. al (Carré, et al., 2013) when concrete samples under compressive load level which corresponded from 0%

up to 40% of the compressive strength of concrete. The applied heating followed the ISO 834 temperature-time curve. As a result of the research, only samples subjected to maximum load level experienced spalling. In the present research under heating conditions which corresponded to the opening factor $O = 0.0415\ m^{1/2}$ spalling occurred under the compressive loading which corresponded to 53% of the maximum compressive strain of concrete. However, the heating rate was lower than that in ISO 834 temperature-curve. But both heating conditions can be considered as "slow" developing curves which resulted in one-time explosive spalling after ~20 minutes of heating in both pieces of research.

4.2 Uncertainties

In the present research samples with dimensions 300×300×220 mm were tested to replicate parts of concrete structures in buildings or concrete linings of tunnels exposed to fire. However, the boundary conditions of the samples were totally different from those in real structures. For example, there were unaccounted convective losses from unexposed faces of samples. Also, the moisture could escape from those faces without any resistance, which would be impossible in a real scenario.

The energy losses from the escape of moisture and its further evaporation were not accounted in the finite difference model which resulted in the deviations from experimental data. Apart from that, radiative and convective losses from the top and side faces were not accounted for in the model as well.

The variations of temperature-dependant properties of concrete were taken as theoretical values from Eurocode. However, it uncertain in which conditions, other than temperature, the concrete shows discussed behaviour. Eurocode offers the two extremes of thermal conductivity without further discussion on the applicability of both. Moreover, the lower and the upper limits of conductivity may be adjusted by National annexes. This makes these values uncertain. The definition of real properties of concrete will be beneficial for the validation of the finite difference heat transfer model.

The stress-strain state of a concrete structure was replicated by means of the application of the eccentric compressive force near the exposed face of a sample. This led to the limitation of the maximum applied loading due to the appearance of shear cracks upon exceeding a certain force. The appearance of such cracks is caused by the absence of

reinforcement in the concrete body and that the inner tensile forces were taken solely by concrete. It should be noted, that it is a very rare occasion when a concrete structure exists without any reinforcement. The reinforcement will not only take the inner tensile forces but also will contribute to spalling due to the bending of rods (Liu, et al., 2018).

Also, a localized area of a concrete structure should be viewed as a restrained body at all sides. In the present experiment, concrete specimens were only partially restrained by the compressive force and the fixing plank in the vertical axis. It means that the material could expand in the other two dimensions without an increase in stress. Experiments performed by other researchers show that those stresses are significant and may lead to the destruction of a sample (Tanibe, et al., 2014) (Boström, et al., 2018).

Due to the fact that concrete is a composite material there is uncertainty in the reproducibility of material properties from test to test. The uneven distribution of aggregate and other components, possible involvement of air bubbles lead to the variability of thermal and mechanical properties. It means that even two samples from the same mix which were cured under the same conditions may show different behavior in such tests. In present research a maximum number of 3 and the average number of 2 samples were tested under the same heating and loading conditions. It means that due to the variability of properties those results may be not replicated in the same way if more samples were tested.

The strains on the front face of concrete samples were controlled by glued strain gauges. However, the higher the load was, the bigger deviations in readings were registered. Such deviations are explained not only by the discussed variabilities in the properties of concrete but also by the small variabilities in the shape of specimens and in the geometry of the set-up e.g. the exact location of the compressive force. Apart from that, the readings received from strain gauges depend on the glue contact between the gauge and the surface. The surfaces of samples were porous and the composition of concrete behind it was uneven with a highly varied distribution of aggregates which eventually influenced the deviations in the readings of strains.

The thermocouples installed in the body of concrete were aligned before the poring of concrete mix into the forms. The process of pouring and further vibrating of forms might have influenced the actual location of thermocouples and the exact location was uncertain in the time of the experiments.

CHAPTER 5. CONCLUSIONS

Experimental research was conducted to study the phenomenon of concrete spalling and the influence of sustained stress and heating conditions on its occurrence.

The negative influence of compressive loading manifested during the research. It was found that the compressive loading which corresponds to 53% of concrete's ultimate strain induces spalling while lower loading does not at the same heating and other conditions. Also, higher compressive loading leads to less time to spalling.

The increase in the rate of heating resulted in the occurrence of spalling under lower compressive loading level. It proves that more severe heating condition are potentially more hazardous in terms of the occurrence of concrete spalling. However, the results of the research showed that "faster" heating of concrete specimens leads to progressive spalling with less damage per one spalling event while "slower" heating resulted in longer time to spalling but in the single deeper one-time damage. Apart from that, the "faster" heating rates require less total energy and less steep temperature gradient for a spalling event to occur. Based on these findings, it can be concluded that both "slow" and "fast" heating regimes should be in the focus of researchers to cover both recognized types of spalling destruction.

Based on the experimental data, general conditions of compressive loading levels and opening factors of parametric temperature-time curves which may lead to the occurrence of spalling of concrete were developed. Also, a common pattern of temperature gradients at the timestamp of spalling has been found. These diagrams can be used by designers and researchers to identify the conditions which should be avoided in order to lower the risk of spalling of concrete.

Another important finding of the research is the substantial influence of ageing of concrete on its propensity to spalling. Samples after 309 days of curing did not experience any spalling while the ones after 146 days spalled under equal heating conditions. Such behaviour is tied with the decrease of the degree of pore saturation (DPS). Based on this, It can be said that additional fire safety measures should be advised during the first year after concrete structures were cast.

The influence of the inclusion of polypropylene fibres in the concrete mix is considered positive in the mitigation of spalling due to the absence of any damage at the most severe

conditions of the experimental research – namely the highest heating rates together with the highest level of compressive loading.

As unloaded concrete structures rarely exist in buildings or tunnels and it was shown that the load does influence the occurrence of spalling, the application of external loading in experimental testing of the propensity of concrete samples to spalling is of high importance. Also, experimental research of concrete samples should not focus only on the most severe heating conditions such as hydrocarbon of RWS temperature-time curves, because "slower" heating rates of parametric fire curves may lead to more severe spalling of the other type, which otherwise will be out of researcher's view.

The properties of concrete such as moisture content, degree of pore saturation and permeability are important factors which should be defined in the research of concrete spalling as opposed to rely solely on moisture content as Eurocode does. Apart from that, it would be beneficial to perform tests on circular-framed samples which help to minimize the effect of scale, unnatural escape of moisture from the sides of samples and which show more realistic internal stresses caused by external loads or restraints.

This page is intentionally left blank

REFERENCES

Arita, F., Harada, K. & Miyamoto, K., 2002. Thermal Spalling of High-Performance Concrete During Fire. *Second International Workshop "Structures in Fire",* 18-19 March.pp. 253-271.

AS 3600:2018, . *AS 3600: Concrete Sctructures,* Sydney, NSW, Australia: SAI Global.

Bailey, C. G., 2002. Holistic behaviour of concrete buildings in fire. *Proceedings of The Institution of Civil Engineers, Structures and Buildings,* 8 1, Volume 152, pp. 199-212.

Bergman, T. L., Lavine, A. S., Incropera, F. P. & Dewitt, D. P., 2016. *Fundamentals of Heat and Mass Transfer, 8th Edition.* New York: Wiley.

Bilodeau, A., Kodur, V. & Hoff, G., 2004. Optimization of the type and amount of polypropylene fibres for preventing the spalling of lightweight concrete subjected to hydrocarbon fire. *Cement and Concrete Composites,* 1 2, 26(2), pp. 163-174.

Boström, L., McNamee, R., Albrektsson, J. & Johansson, P., 2018. *Screening test methods for determination of fire spalling of concrete.* Borås: RISE - Research Institutes of Sweden, Safety and Transport, Safety..

Breunese, A. J., Both, I. C. & Wolsink, G. M., 2008. *2008-Efectis-R0695. Fire testing procedure for concrete tunnel linings,* Bleiswijk: Ministry of Infrastructure and the Environment (Rijkswaterstaat).

BS EN 1991-1-2:2002, . *Eurocode 1:Actions on structures. Part 1-2: General actions – Actions on structures exposed to fire,* : British Standard.

BS EN 1992-1-1:2004+A1:2014, . *Eurocode 2: Design of concrete structures — Part 1-1: General rules and rules for buildings,* : British Standard.

BS EN 1992-1-2:2004, . *Eurocode 2: Design of concrete structures. Part 1-2: General rules — Structural fire design,* : British Standard.

Buch, S. & Kumar Sharma, U., 2019. Fire Resistance of Eccentrically Loaded Reinforced Concrete Columns. *Fire Technology,* 22 2.pp. 1-36.

Building Regulation 2010, 2013. *Approved Document B. Fire safety. Volume 2 - Buildings other than dwllings,* : HM Government.

Carré, H. et al., 2013. Effect of compressive loading on the risk of spalling. *MATEC Web of Conferences,* 2, Volume 6, p. 1007.

Casey, N., 2017. Fire incident data for Australasian road tunnels. *16th Australasian Tunnelling Conference 2017: Challenging Underground Space : Bigger, Better, More,* pp. 560-567.

Choe, G. et al., 2019. Effect of moisture migration and water vapor pressure build-up with the heating rate on concrete spalling type. *Cement and Concrete Research,* 1 2, Volume 116, pp. 1-10.

Choinska, M., Khelidj, A., Chatzigeorgiou, G. & Pijaudier-Cabot, G., 2007. Effects and interactions of temperature and stress-level related damage on permeability of concrete. *Cement and Concrete Research,* 1 1, 37(1), pp. 79-88.

CTIF Center of Fire Statistics, 2019. *Report #24. World Fire Statistics,* Ljubljana, Slovenia: Internation Associacion of Fire and Rescue Services.

Deeny, S. et al., 2008. Spalling of concrete: Implications for structural performance in fire. *University of Canterbury. Civil and Natural Resources Engineering,* pp. 1-5.

Drysdale, D., 2011. *An Introduction to Fire Dynamics.* Chichester: John Wiley & Sons, Ltd.

Gawin, D., Pesavento, F. & Castells, A. G., 2018. On reliable predicting risk and nature of thermal spalling in heated concrete. *Archives of Civil and Mechanical Engineering,* 9, 18(4), pp. 1219-1227.

Hedayati, M., Sofi, M., Mendis, P. & Ngo, T., 2015. A comprehensive review of spalling and fire performance of concrete members. *Electronic journal of structural engineering,* 15(1), pp. 8-34.

Hoseini, M., Bindiganavile, V. & Banthia, N., 2009. The effect of mechanical stress on permeability of concrete: A review. *Cement and Concrete Composites,* 1 4, 31(4), pp. 213-220.

Jansson, R. & Boström, L., 2013. Factors influencing fire spalling of self compacting concrete. *Materials and Structures,* 22 10, 46(10), pp. 1683-1694.

Khoury, G. A., 2008. Polypropylene fibres in heated concrete. Part 2: Pressure relief mechanisms and modelling criteria. *Magazine of Concrete Research,* 25 4, 60(3), pp. 189-204.

Khoury, G. A. & Anderberg, Y., 2000. *Concrete Spalling Review.* Borlänge: Swedish National Road Administration.

Kim, H.-J., Kim, H.-Y., Lee, J.-S. & Kwan, K.-H., 2011. An Experimental Study on Thermal Damage and Spalling of Concrete Under Loading Conditions in a Tunnel Fire. *Journal of Asian Architecture and Building Engineering,* 24 11, 10(2), pp. 375-382.

Liu, J.-C., Tan, K. H. & Yao, Y., 2018. A new perspective on nature of fire-induced spalling in concrete. *Construction and Building Materials,* 30 9, Volume 184, pp. 581-590.

Li, Y., Pimienta, P., Pinoteau, N. & Tan, K. H., 2019. Effect of aggregate size and inclusion of polypropylene and steel fibers on explosive spalling and pore pressure in ultra-high-performance concrete (UHPC) at elevated temperature. *Cement and Concrete Composites,* 1 5, Volume 99, pp. 62-71.

Li, Y., Tan, K. H. & Yang, E.-H., 2018. Influence of aggregate size and inclusion of polypropylene and steel fibers on the hot permeability of ultra-high performance concrete (UHPC) at elevated temperature. *Construction and Building Materials,* 30 4, Volume 169, pp. 629-637.

Lo Monte, F., Felicetti, R. & Rossino, C., 2019. Fire spalling sensitivity of high-performance concrete in heated slabs under biaxial compressive loading. *Materials and Structures,* 25 2, 52(1), p. 14.

Loo, Y. H., 1992. A new method for microcrack evaluation in concrete under compression. *Materials and Structures,* 12, 25(10), pp. 573-578.

Loo, Y. H., 1995. Propagation of microcracks in concrete under uniaxial compression. *Magazine of Concrete Research,* 25 3, 47(170), pp. 83-91.

Maluk, C., 2014. *Development and application of a novel test method for studying the fire behaviour of CFRP prestressed concrete structural elements,* Edinburgh: The University of Edinburgh.

Maluk, C., Bisby, L. & Terrasi, G. P., 2017. Effects of polypropylene fibre type and dose on the propensity for heat-induced concrete spalling. *Engineering Structures,* 15 6, Volume 141, pp. 584-595.

Ma, Q. et al., 2015. Mechanical properties of concrete at high temperature—A review. *Construction and Building Materials,* 15 9, Volume 93, pp. 371-383.

Maraveas, C. & Vrakas, A. A., 2014. Design of Concrete Tunnel Linings for Fire Safety. *Structural Engineering International,* 23 8, 24(3), pp. 319-329.

Memon, S. A., Shah, S. F. A., Khushnood, R. A. & Baloch, W. L., 2019. Durability of sustainable concrete subjected to elevated temperature – A review. *Construction and Building Materials,* 28 2, Volume 199, pp. 435-455.

Mendis, P., Nguyen, K. & Ngo, T., 2014. Fire design of high strength concrete walls. *Concrete in Australia,* 1 1, Volume Volume 40, pp. 38-43.

Miah, M. et al., 2016. Fire spalling behaviour of concrete: Role of mechanical loading (uniaxial and biaxial) and cement type. *Key Engineering Materials,* 23 9, Volume 711, pp. 549-555.

Ministère de l'Equipement, 2000. *Instruction technique annexée à la Circulaire interministérielle no 2000-63 du 25 Aout 2000 relative à la sécurité dans les tunnels du réseau routier français.,* Paris: Bulletin officiel du Ministère de l'Equipement n°0 20000-6 du 01 09 2000.

Missemer, L. et al., 2019. Fire spalling of ultra-high performance concrete: From a global analysis to microstructure investigations. *Cement and Concrete Research,* 1 1, Volume 115, pp. 207-219.

Novak, J. & Kohoutkova, A., 2018. Mechanical properties of concrete composites subject to elevated temperature. *Fire Safety Journal,* 1 1, Volume 95, pp. 66-76.

Ozawa, M., Uchida, S., Kamada, T. & Morimoto, H., 2012. Study of mechanisms of explosive spalling in high-strength concrete at high temperatures using acoustic emission. *Construction and Building Materials,* 1 12, Volume 37, pp. 621-628.

Phan, L. T., 2008. Pore pressure and explosive spalling in concrete. *Materials and Structures,* 18 12, 41(10), pp. 1623-1632.

Phan, L. T. & Carino, N. J., January-February 2002. Effects of Test Conditions and Mixture Proportions on Behavior of High-Strength Concrete Exposed to High Temperatures. *ACI Materials Journal,* 99(1), pp. 54-66.

Phan, M. et al., 2011. A finite element modeling of thermo-hydro-mechanical behavior and numerical simulations of progressing spalling front. *Procedia Engineering,* 1 1, Volume 10, pp. 3128-3133.

RABT 02, 2002. *RABT Guidelines for equipment and operation of road tunnels (Richtlinien für die Ausstattung und den Betrieb von Strassentunneln) Forschungsgesellschaft für Strassen- und Verkehrswesen. (Road and Transportation Research Association),* Köln: FGSV-Verlag.

Ren, R. et al., 2019. Statistical analysis of fire accidents in Chinese highway tunnels 2000–2016. *Tunnelling and Underground Space Technology,* 1 1, Volume 83, pp. 452-460.

Rickard, I., Bisby, L., Deeny, S. & Maluk, C., 2016. Predictive testing for heat induced spalling of concrete tunnels – The influence of mechanical loading. *International Conference on Structures in Fire,* pp. 1-8.

Rickard, I., Gerasimov, N., Bisby, L. & Deeny, S., 2017. Predictive testing for heat induced spalling of concrete tunnel linings – The potential influence of sustained mechanical loading. *5th International Workshop on Concrete Spalling due to Fire Exposure, 12-13 October 2017, Borås, Sweden,* pp. 337-344.

Sanjuán, M. A. & Muñoz-Martialay, R., 1995. Influence of the age on air permeability of concrete. *Journal of Materials Science,* 30(22), pp. 5657-5662.

Tanibe, T., Ozawa, M., Kamata, R. & Rokugo, K., 2014. Steel Ring-Based Restraint of HSC Explosive Spalling in High Temperature Environments. *Journal of Structural Fire Engineering,* 1 9, Volume 5, pp. 239-250.

Thorne, T., 2018. *Mechanisms of Fire-Induced Concrete Spalling,* Brisbane: The Univesity Of Queensland.

Voeltzel, A. & Dix, A., 2004. A comparative analysis of the Mont-Blanc, Tauern and Gothard tunnel fires. *Routes & Roads,* 10, Volume 324, pp. 18-34.

Wang, G., Barber, D., Johnson, P. & Hui, M.-C., 2013. Fire Safety Provisions for Aged Concrete Building Structures. *Procedia Engineering,* 1 1, Volume 62, pp. 629-638.

Wong, H., Zobel, M., Buenfeld, N. & Zimmerman, R., 2009. Influence of the interfacial transition zone and microcracking on the diffusivity, permeability and sorptivity of cement-based materials after drying. *Magazine of Concrete Research,* 25 10, 61(8), pp. 571-589.

Wyrzykowski, M., McDonald, P. J., Scrivener, K. L. & Lura, P., 2017. Water Redistribution within the Microstructure of Cementitious Materials due to Temperature Changes Studied with 1 H NMR. *The Journal of Physical Chemistry C,* 21 12, 121(50), pp. 27950-27962.

Yang, J. & Peng, G. F., 2010. The Mechanism of Explosive Spalling and Measures to Resistant Spalling of Concrete Exposed to High Temperature by Incorporating Fibers: A Review. *Advanced Materials Research,* 12, Volume 168-170, pp. 773-777.

Zhang, Y., Zeiml, M., Pichler, C. & Lackner, R., 2014. Model-based risk assessment of concrete spalling in tunnel linings under fire loading. *Engineering Structures,* 15 10, Volume 77, pp. 207-215.

Zhao, J., Zheng, J.-J., Peng, G.-F. & van Breugel, K., 2017. Numerical analysis of heating rate effect on spalling of high-performance concrete under high temperature conditions. *Construction and Building Materials,* 10, Volume 152, pp. 456-466.

ZTV - Tunnel, 1995, 1999. *ZTV Additional Technical Conditions for the Construction of Road Tunnels (Zusätzlichen Technischen Vertragsbedingungen und Richtlinien für den Bau von Strassentunneln). Forschungsgesellschaft für Strassen- und Verkehrswesen.,* Dortmund: Verkehrsbl.-Verl..

APPENDIX A

Sample label	Mixture Type	Opening factor	Compressive force	TC Depth [mm] [1]
HC0.0415_L53%_PP0.0	Plain concrete	0.0415	400 kN	10
				30
				50
HC0.0415_L19%_PP0.0	Plain concrete	0.0415	160 kN	10
				30
				50
HC0.0415_L53%_PP0.0_1	Plain concrete	0.0415	400 kN	10
				30
				50
HC0.0415_L53%_PP0.0_2	Plain concrete	0.0415	400 kN	30
				30
				50
HC0.0415_L0%_PP0.0	Plain concrete	0.0415	No load	10
				30
				50
HC0.0415_L0%_PP0.0_1	Plain concrete	0.0415	No load	- [2]
HC0.0415_L40%_PP0.0	Plain concrete	0.0415	280 kN	10
				30
				50
HC0.0515_L0%_PP0.0	Plain concrete	0.0515	No load	10
				30
				50
HC0.0515_L40%_PP0.0	Plain concrete	0.0515	280 kN	- [2]
HC0.1_L40%_PP0.0	Plain concrete	0.1	280 kN	7
				27
				50
HC0.1_L19%_PP0.0	Plain concrete	0.1	160 kN	- [2]
HC0.1_L40%_PP0.0_1	Plain concrete	0.1	280 kN	7
				27
				50
HC0.1_L40%_PP1.6	1.6 kg/m³ PP	0.1	280 kN	7
				30
				50
HC0.1_L53%_PP1.6	1.6 kg/m³ PP	0.1	400 kN	- [2]
HC0.2_L53%_PP1.6	1.6 kg/m3 PP	0.2	400 kN	10
				20
				30
HC0.1_L53%_PP1.6_1	1.6 kg/m³ PP	0.1	400 kN	7
				30
				50
HC0.2_L53%_PP1.6_1	1.6 kg/m³ PP	0.2	400 kN	- [2]
HC0.1_L40%_PP1.6_1	1.6 kg/m³ PP	0.1	280 kN	10
				30
				50

[1] Measurement of thermocouple depth from exposed surface was conducted at time of casting

[2] Thermocouples not provided